Arteriosclerosis, Thrombosis, and Vascular Biology

BASIC SCIENCES

Runx2 (Runt-Related Transcription Factor 2) Links the DNA Damage Response to Osteogenic Reprogramming and Apoptosis of Vascular Smooth Muscle Cells

Andrew M. Cobb, Syabira Yusoff, Robert Hayward, Sadia Ahmad, Mengxi Sun, Anja Verhulst, Patrick C. D'Haese, Catherine M. Shanahan

OBJECTIVE: The development of ectopic vascular calcification is strongly linked with organismal aging, which is primarily caused by the accumulation of DNA damage over time. As Runx2 (Runt-related transcription factor 2) has been identified as a regulator of vascular smooth muscle cell osteogenic transition, a key component of vascular calcification, we examined the relationship between DNA damage and Runx2 activation.

APPROACH AND RESULTS: We found genotoxic stress-stimulated Runx2 accumulation and transactivation of its osteogenic target genes, leading to enhanced calcification. Inhibition of DNA damage signaling attenuated this response. Runx2 localized to sites of DNA damage and participated in DNA repair by regulating phosphorylation events on histone H2AX, with exogenous expression of Runx2 resulting in unrepaired DNA damage and increased apoptosis. Mechanistically, Runx2 was PARylated in response to genotoxic stress, and inhibition of this modification disrupted its localization at DNA lesions and reduced its binding to osteogenic gene promoters.

CONCLUSIONS: These data identify Runx2 as a novel component of the DNA damage response, coupling DNA damage signaling to both osteogenic gene transcription and apoptosis and providing a mechanism for accelerated mineralization in aging and chronic disease.

GRAPHIC ABSTRACT: A graphic abstract is available for this article.

Key Words: aging ■ apoptosis ■ DNA damage ■ poly ADP ribosylation ■ vascular calcification

Ectopic vascular calcification invariably increases with age and is a major risk factor for cardiovascular mortality.[1–3] It is a cell-mediated process driven by vascular smooth muscle cells (VSMCs)[4,5] that ordinarily are essential for maintaining vascular tone through their contractile activity. However, in aging and disease, these cells display marked phenotypic plasticity and can undergo osteochondrogenic differentiation. This transition is characterized by a loss of contractile markers[6] and increased expression of osteogenic factors including the master transcription factor Runx2 (Runt-related transcription factor 2) and its downstream osteogenic targets Osterix,[7] OCN (osteocalcin),[8] and BSP (bone sialoprotein).[9–11] Increased secretion of calcifying vesicles[12] and a higher incidence of

See accompanying editorial on page 1358

Correspondence to: Catherine M. Shanahan, PhD, James Black Centre, 125 Coldharbour Land, London SE5 9NU, United Kingdom, Email cathy.shanahan@kcl.ac.uk; or Andrew M. Cobb, PhD, BHF Centre of Research Excellence, School of Cardiovascular Medicine and Sciences, King's College London, The James Black Centre, United Kingdom, Email andrew.cobb@kcl.ac.uk

The Data Supplement is available with this article at https://www.ahajournals.org/doi/suppl/10.1161/ATVBAHA.120.315206.

For Sources of Funding and Disclosures, see page 1356.

Arterioscler Thromb Vasc Biol is available at www.ahajournals.org/journal/atvb

Nonstandard Abbreviations and Acronyms

γH2AX	phosphorylation of histone H2AX on serine 139
ATM	ataxia-telangiectasia mutated
BBPDA	boronate bead pull-down assay
BSP	bone sialoprotein
CC3	cleaved caspase-3
CKD	chronic kidney disease
DDR	DNA damage response
EGFP	enhanced green fluorescent protein
FL-Runx2	recombinant FLAG-tag Runx2
JNK	c-Jun N-terminal protein kinase
KO	knockout
MEK	mitogen-activated protein kinase
OCN	osteocalcin
PAR	poly(ADP-ribose)
PARG	poly(ADP-ribose) glycohydrolase
PARP	poly(ADP-ribose) polymerase
PCR	polymerase chain reaction
pY142-H2AX	phosphorylated tyrosine 142 on H2AX
Runx2	Runt-related transcription factor 2
shRunx2	short hairpin RNA against Runx2
Tk	thymidine kinase
VitD	vitamin D
VSMC	vascular smooth muscle cell
WB	Western blot

Highlights

- DNA damage accelerates calcification of vascular smooth muscle cells, and this is dependent on Runx2 (Runt-related transcription factor 2).
- DNA damage induces PARylation of Runx2, and this requires both ATM (ataxia-telangiectasia mutated) and PARP (poly[ADP-ribose] polymerase) activity.
- PARylation of Runx2 results in its accumulation and subsequent increase in expression of osteogenic target genes, as well as localization to sites of DNA damage.
- At DNA lesions, Runx2 plays a direct role in the DNA damage response by promoting retention of phosphorylated tyrosine 142 on H2AX and promoting apoptosis in favor of DNA repair.
- Osteogenic transition and apoptosis of vascular smooth muscle cells work in concert to drive vascular calcification during aging.

apoptosis[13,14] are also recognized features of this osteogenic switch, which orchestrates the calcification process. However, the specific pathways that link these processes with aging have remained elusive.

Runx2 is essential for developmental osteogenesis in bone,[15,16] but it has functions beyond activation of osteogenic transcriptional programmes and is expressed in a number of nonmineralizing cell types.[17] In the vasculature, Runx2 is upregulated at sites of calcification, and targeted KO (knockout) of Runx2 reduces expression of its osteogenic targets and reduces calcification.[18–21] Notably, however, Runx2 is transiently upregulated in the absence of calcification at sites of vascular injury[22] while targeted overexpression of Runx2 in VSMCs in vivo is insufficient for calcification to ensue[23] suggesting that additional factors or modifications are required to activate its osteogenic capacity.

Runx2 acts as a scaffold to organize enhancers and repressors, and its transcriptional activity is dependent on its localization to the nuclear matrix.[24,25] This proteinaceous network acts to organize nuclear metabolic events, including transcription and the DNA damage response (DDR),[26–28] and emerging evidence suggests that Runx2 may have a direct function in the DDR,[24,29] with its deregulation in a range of cancers further substantiating this notion.[30–32] Importantly, DDR regulators are also instrumental during normal physiological bone formation and in ectopic vascular calcification,[33–35] suggesting a link between Runx2 activity, DNA damage repair, and osteogenesis.

A primary event in the DDR is phosphorylation of histone H2AX on serine 139 (γH2AX) by the kinase ATM (ataxia-telangiectasia mutated),[36] and cells positive for γH2AX are detectable in the bone growth plate and in calcified arteries.[35] In addition, ATM and DDR effector proteins c-Abl and p53 have been shown to regulate osteoblast activity.[37,38] Another key DDR component is PARP (PAR [poly(ADP-ribose)] polymerase) signaling. This pathway, usually activated by oxidative stress, involves the posttranslational addition of PAR moieties, by PARP enzymes, to target proteins in a process termed PARylation. PARP1 has been shown to play a role in osteogenic differentiation in bone,[39] and high levels of PAR have been detected in the bone growth plate and at sites of vascular calcification.[35,40,41] PAR itself can avidly bind calcium and form calcified nanoparticles, suggesting a byproduct of the DDR is also essential for biomineralization.[35] Inhibitors of DDR signaling can block osteogenic differentiation and calcification in both bone and the vasculature; however, the mechanisms behind this remain unclear.[33,35]

In this study, we hypothesized that DDR signaling might activate Runx2-mediated osteogenesis in the vasculature. Using in vitro and in vivo models of Runx2 depletion and overexpression, we show that Runx2 is a novel component of the DDR that regulates H2AX phosphorylation in response to DNA damage and promotes apoptosis. PARylation of Runx2 was essential for this activity and for its activation of osteogenic gene expression in VSMCs. We have outlined a precise role for

Runx2 during the DDR, and our data provide an explanation for the increased incidence of vascular calcification observed with age and highlight the potential for DDR inhibitors as therapeutics for vascular calcification.

MATERIALS AND METHODS

The authors declare that all supporting data are available within the article (and its Data Supplement).

Cell Culture/Treatments

VSMCs were obtained from explants of human aortic tissues from both male and female donors of various ages as described previously.[42] The isolates used in this study were as follows; 35F (04:35F:11A), 20M (05:20M:18A), and 54M (05:54M:20). Cells were maintained in M199 medium (Sigma-Aldrich) supplemented with 20% fetal bovine serum at 37 °C and 5% CO_2 and used between passages 9 and 20. Control mouse VSMCs (*Runx2*$^{f/f}$) and Runx2 KO VSMCs (*Runx2*$^{\Delta SM}$) were cultured in the same media. To induce calcification, VSMCs were cultured in M199 medium supplemented with 5% fetal bovine serum and elevated calcium (Ca^{2+}) and phosphate (P_i; 2.7 and 2.5 mmol/L, respectively) for between 8 and 15 days until signs of calcification became apparent. Control medium was M199 with 5% fetal bovine serum and no additional Ca^{2+} or P_i (1.8 and 1 mmol/L, respectively). For short-term DNA damage induction, cells were typically treated for 0.5 to 3 hours with 20 µmol/L etoposide or 200 mmol/L H_2O_2. For long-term treatments performed alongside calcification experiments (>24 hours), concentrations of 5 µmol/L etoposide or 20 mmol/L H_2O_2 were used. Inhibitors against PARP, ATM, and MEK (mitogen-activated protein kinase; PJ34 [AdipoGen], KU55933 [Selleckchem], U0126 [Sigma-Aldrich], respectively) were used at 10 µmol/L. DMSO (dimethyl sulfoxide) was used as a vehicle control.

Generation of Conditional Runx2 KO Mice

The conditional Runx2 KO mouse model was generated by Taconic Artemis. The targeting strategy was based on the Ensembl transcript ENSMUST00000160673 (Runx2-001), which allows conditional KO of the Runx2 gene (*Runx2*). The *Runx2* targeting vector was created by flanking the *Runx2* targeted domain of exon 4 with *loxP* sites, and the positive selection marker puromycin resistant was flanked by flippase recognition target sites. The targeting vector was generated using bacterial artificial chromosome clones from C56LB/6J RPCIB-731 bacterial artificial chromosome library. The target vector was injected into embryonic stem cells from Taconic Artemis C57BL/6 N by electroporation, and cells with successful homologous recombination were isolated using positive (puromycin resistant) and negative (Tk [thymidine kinase]) selections. These were injected into C57BL/6 mouse blastocysts to generate chimeric floxed-Runx2 mice, which were then bred onto a flippase recombinase strain to remove the puromycin cassette. To generate smooth muscle cell–specific Runx2 KO mice (*Runx2*$^{\Delta SM}$), *Runx2*$^{f/f}$ mice were crossed with mice expressing smooth muscle cell–specific Cre recombinase, which is driven by the SM22-α promoter. The SM22 Tg(Tagln-cre)1Her/J mice (004746; The Jackson Laboratory). Genotyping was performed using polymerase chain reaction (PCR) of DNA extracted from ear biopsy specimens. Primers used for genotyping were as follows: Runx2 conditional KO: forward, 5′ GAGCTAGCCTAGCCTTTCTGC 3′ and reverse, 5′ CAAGAGGACTCAAGTTCAGATCC 3′. Cre recombinase expression: forward, 5′ GCGGTCTGGCAGTAAAAACTATC 3′ and reverse, 5′ GTGAAACAGCATTGCTGTCACTT 3′. Cycling parameters were the following: initial denaturation 95 °C, 5 minutes; denaturation 95 °C, 30 seconds (repeated for 35 cycles); annealing 60 °C, 30 seconds (repeated for 35 cycles); extension 72 °C, 1 minute (repeated for 35 cycles); final extension 72 °C, 10 minutes; cooled to 4 °C indefinitely. The PCRs produced amplicons of 197 (wild-type allele), 354 (conditional KO allele), and 100 bp (Cre recombinase). *Runx2*$^{f/f}$ and *Runx2*$^{\Delta SM}$ mice were maintained on a C57BL/6 background. All mice were kept in individually ventilated cages at the biological services unit at the Maurice Wohl Clinical Neuroscience Institute, King's College London. They were maintained on a normal diet (LabDiet 5053/PicoLab Rodent Diet 20) and kept on a 12-hour light/dark cycle. Male and female mice were used in this study. All experiments were performed in accordance with the UK Animal (Scientific Procedures) Act 1986 and were covered by a Home Office project license.

Vitamin D Induction of Calcification in Mice

Vitamin D (VitD) treatment is an established model used to induce vascular calcification in mice. It causes dysregulation of calcium metabolism, resulting in increased serum calcium but unchanged phosphate levels.[43] For this treatment, Cholecalciferol (C1357; Sigma) was dissolved in 100% ethanol and diluted to 1.25 µg/µL containing 5% ethanol for each injection. Twenty-week-old *Runx2*$^{f/f}$ and *Runx2*$^{\Delta SM}$ mice on a C57BL/6 background received cholecalciferol subcutaneously at a dosage of 500 000 IU/kg per day for 4 consecutive days, and 5% ethanol in sterile water was used as vehicle control.[18] The mice were monitored daily and terminated between 7 and 8 days after injection. Thoracic aortas were collected for calcium quantification, RNA, and histology. Male and female mice were used to comply with 3R policy to reduce animal use, and data were pooled for analysis.

Rat Model With Chronic Kidney Disease Induced Vascular Calcification

This study used a well-characterized rat model with adenine-induced chronic kidney disease (CKD).[35,44] Seven-week-old male Wistar rats (225–250 g; Charles River, Lille, France) were used to avoid interference with hormonal effects and because they are more vulnerable to the development of CKD. Rats were housed 2 per cage and randomly assigned to different groups. An equilibration period of 3 weeks was used to ensure a body weight of ≈320 g at the start of the study. CKD was induced by maintaining the rats on an adenine diet containing 0.75% adenine (Acros Organics) with a 0.92% phosphorous and 1% calcium content in combination with a low protein content (2.5%). A control group (n=6) with normal renal function was included and maintained on a control diet. The CKD groups were euthanized weekly starting from week 1 and then 2, 3, 4, and 8 after the diet was introduced. The control group rats with normal diet were euthanized at the end of the experiment (week 8).

Adenoviral Constructs and Transfections

Adenovirus (Cyagen Biosciences) expressing FL-Runx2 (recombinant FLAG-tag Runx2), a shRunx2 (short hairpin RNA against Runx2) mRNA, or EGFP (enhanced green fluorescent protein) were used to transduce VSMCs at 70% confluence. Multiplicity of infection was 10 particles per cell, routinely achieving >80% transduction efficiency as assessed by control EGFP. For small interfering RNA–mediated interference of Ku70, sc29383 (Santa Cruz Biotech) was transfected into VSMCs using HiPerfect transfection reagent (Qiagen).

Antibodies

Primary antibodies used were as follows: Runx2 (D130-3; MBL International); Runx2 (sc-10758), p53 (sc-126; Santa Cruz Biotech); FLAG (M2, F3165), H2AX (PLA0294), β-actin (AC-74; Sigma-Aldrich); 8-OxodG (N45.1; JalCA); FLAG (ab1257), Ku70 (ab83501), ERK 1/2 (extracellular signal-regulated kinase; ab36991), pERK (ab201015), phosphorylated tyrosine 142 on H2AX (pY142-H2AX; ab94602), α-smooth muscle actin (ab7817), Runx2 (ab23981; Abcam); γH2AX (2577), lamins A/C (2032), Chk2 (checkpoint kinase 2; 2662), pChk2 (phospho-Chk2; T68; 2197), CC3 (cleaved caspase-3; Asp175; 9661; Cell Signaling Technology, Danvers, MA); PAR (4336-APC-050; Novus Biologicals).

TUNEL Staining

TUNEL (terminal deoxynucleotidyl transferase dUTP nick-end labeling) staining assays were performed using a commercially available kit according to the manufacturer's instructions (Abcam; ab206386).

Calcification Assays

For Alizarin red S staining, VSMCs were washed with PBS and fixed in 4% formaldehyde in PBS for 10 minutes at 21 °C. VSMCs were then washed with dH_2O and then incubated with 2% Alizarin red S (Sigma-Aldrich) for 5 minutes, then briefly rinsed with water before imaging. o-Cresolphthalein assays on VSMCs were performed as described previously.[42] Adenovirus was used to knock down Runx2 (shRunx2), overexpress Runx2 (FL-Runx2), or express EGFP (control). To harvest cells from mouse models, 3 mm of thoracic aorta for each mouse was collected and washed in Hank's balanced salt solution. To extract Ca^{2+}, the aortas were placed in a Dounce Glass Tissue Homogenizer with 200 µL 0.1 M HCl and homogenized every 30 minutes for 2 hours. The homogenate was centrifuged at 13 000*g* for 2 minutes and subject to o-Cresolphthalein assay for calcium analysis.

Immunoblotting

Total cell extracts were prepared by washing VSMCs in ice-cold PBS, then scraping into fresh ice-cold PBS and centrifugation at 700*g* for 5 minutes. Pellets were resuspended in lysate buffer (10 mmol/L Tris pH 7.5, 150 mmol/L NaCl, 1 mmol/L EDTA, 1% Triton X-100, protease inhibitors) and sonicated for 10 seconds followed by centrifugation at 700*g* for 5 minutes. 0.01% bromophenol blue, 200 mmol/L DTT, 4% SDS, and 20% glycerol were added to lysates before boiling for 5 minutes and separation by SDS-PAGE, transfer to PVDF (polyvinylidene fluoride) membrane, blocking, and primary antibody incubation. Secondary antibodies conjugated to IRDye 800CW (LI-COR Biosciences) were then used followed by detection and quantification with an imager (Odyssey; LI-COR Biosciences).

Immunofluorescence

VSMCs were cultured on coverslips and fixed in 4% paraformaldehyde in PBS for 10 minutes at 21 °C followed by 3-minute permeabilization with 0.5% NP-40 in PBS. Coverslips were then blocked (3% BSA in PBS) for 1 hour at 21 °C before incubation with primary antibodies in blocking solution for 12 hours at 4 °C in a humidifying chamber. Coverslips were washed in PBS followed by 1-hour 21 °C incubation with fluorescent dye conjugated secondary antibodies (Invitrogen). Coverslips were washed with PBS, mounted onto slides with medium containing DAPI (4′,6-diamidino-2-phenylindole), and z stacks were obtained using a Nikon A1R confocal microscope with NIS-Elements software. Different channels were acquired sequentially. For mice thoracic aortas, 10-µm-thick cryosections were stained and imaged using an Olympus IX-81 microscope.

Comet Assays

VSMCs were cultured to ≈70% confluency and then were washed with ice-cold PBS, trypsinised, and resuspended in 0.6% low melting point agarose and then dispensed in duplicate onto precoated slides and allowed to set on ice for 20 minutes in the dark. Slides were then transferred into ice-cold lysis buffer (100 mmol/L EDTA, 2.5 M NaCl, 10 mmol/L Tris pH10, and 1% Triton X-100) for 1 hour, washed twice with ice-cold dH_2O followed by electrophoresis in ice-cold buffer (300 mmol/L NaOH and 1 mmol/L EDTA) at 20 V for 30 minutes. Slides were then submerged in neutralization buffer (0.4 M Tris pH 7.5), washed with dH_2O, and dried before staining with Nancy-520 (Sigma-Aldrich) and imaging by confocal microscopy.

Immunohistochemistry

Immunohistochemistry was performed on Wistar rat thoracic aortas. Four- or 7-µm thick sections were paraffinized, rehydrated, restored for immunoreactivity, blocked for endogenous peroxidase activity and nonspecific binding, and then were incubated with primary antibodies. The biotinylated secondary antibodies, avidin-biotin complex amplification (PK-6101 and PK-6102; Vector Laboratories), and DAB (3,3'-diaminobenzidine) peroxidase substrate kit (SK-4100; Vector Laboratories) were used to develop the staining. Sections were then counterstained with hematoxylin and mounted using DPX (distyrene, a plasticizer, and xylene) following dehydration. Images were taken using a Leica ICC50 W microscope. Mineral deposition and expression of γH2AX, 8-oxodG, and Runx2 were quantified using ImageJ software. Calcification was quantified using a threshold measure method and expression of γH2Ax, 8-oxodG, and Runx2 by enumerating positive (brown) and negative (purple) cells.

RNA Isolation and Quantitative Reverse Transcription Polymerase Chain Reaction

RNA from human VSMCs was isolated from cells using STAT60 (CS-110; AMS Biotechnology), followed by cDNA

synthesis using Mu-MLV reverse transcriptase (ME-0125-10; Eurogentec). qPCR (quantitative PCR) was performed in triplicate using qPCRBIO SyGreen Mix (PCR Biosystems). Reactions were performed in a StepOnePlus Real Time PCR System (Applied Biosystems). Primers used are as follows: *Runx2* (Runx2; QT00020517), *CDKN1A* (p21; QT00062090), *GAPDH* (GAPDH; QT00079247), *Sp7* (Osterix; QT00213514), and *MMP9* (MMP9; QT00040040; Qiagen). Other primers used were *BGLAP* (OCN; 5′-GGCAGCGAGGTAGTGAAGAG-3′ and 5′-CGATAGGCCTCCTGAAAGC-3′) and *IBSP* (BSP; 5′-AGTTTCGCAGACCTGACATCCAGT-3′ and 5′-TTCATAACTG TCCTTCCCACGGCT-3′). Expression levels of target genes were all corrected using GAPDH expression. PCRs were performed in 20 µL reaction volumes at 95°C for 10 minutes followed by 40 cycles at 95°C for 5 seconds and 60°C for 1 minute. RNA was extracted from mouse aorta by homogenizing vessels in 1 mL TRIzol (Invitrogen) using matrix D beads (MP Biomedicals) in a Precellys 24 tissue homogenizer (Bertin Technologies). cDNA synthesis and qPCR were performed as described above but using the following primers: *Runx2* (QT00102193), *GAPDH* (QT01658692), *IBSP* (QT00115304), *Sp7* (QT00293181), and BGLAP (QT01744330; Qiagen).

Proximity Ligation Assay

Duolink In Situ Red Starter Kit Mouse/Rabbit (Sigma-Aldrich) was used according to the manufacturer's instructions. Staining was visualized using a Nikon A1R confocal microscope.

Active Caspase 3 ELISA

Active caspase 3 (Asp175) human ELISA (ab168541; Abcam) was performed according to the manufacturer's instructions.

Chromatin Immunoprecipitation

ab500 ChIP Kit (Abcam) was used according to the manufacturer's instructions. Briefly, VSMCs were trypsinised, centrifuged, and then washed in ice-cold PBS. Cells were centrifuged again and then fixed in 1.1% formaldehyde in PBS. Reactions were quenched with glycine, and cells were washed in ice-cold PBS before being lysed. Chromatin was sheared to ≈500- to 1500-bp fragments using a sonicator at 4°C. Chromatin was diluted, and input chromatin was collected. Remaining chromatin was used for chromatin immunoprecipitation using 4 µg Runx2 (D130-3) as antibody of interest, 4 µg anti-histone H3 as a positive control, and no antibody as a negative control. Antibodies were added for 12 hours at 4°C, and then protein A sepharose beads were used to precipitate protein/DNA complexes. Cross-links were reversed by heating at 98°C followed by proteinase K addition and DNA purification. Samples were analyzed by pPCR. Primers used are as follows: Runx2 (5′-TGTGATACAGTCCAAAGATGTGA-3′ and 5′-CCTGTAAGGTTAAGCATTTGTAGAG-3′), p21 (5′-TGCT AGGAACATGAGCAAACT-3′ and 5′-TCAGCAGTGGCACAATC TC-3′), BSP (5′-GGGCCACATAAATGGACAATA-3′ and 5′-TCA TTTGATGTTTCCTCCTGAA-3′), Osterix (5′-CCTTGCCTATCTGC TTCTCTTT-3′ and 5′-GTCCTGGATCCAAGCTTCAAA-3′), MMP9 (5′-CCAATCACCACCATCCGTT-3′ and 5′-ACAGCAGACATGG CTTTACTC-3′), and OCN (5′-AAATACAGAATTAGCCAGGCAT-3′ and 5′-AAGAAGCAAGAGAAACAAAGTG-3′).

Biochemical Fractionation

VSMCs were incubated in fractionation buffer (10 mmol/L HEPES pH 7.9, 10 mmol/L KCl, 1.5 mmol/L $MgCl_2$, 0.5 mmol/L DTT, 0.05% NP-40, protease inhibitors, and phosphatase inhibitors) on ice for 30 minutes with occasional agitation. Following centrifugation at 1500*g* for 5 minutes at 4°C, the supernatant was collected (cytoplasmic) and the pellet was extracted with ice-cold high-salt buffer (20 mmol/L Tris-HCl [pH 8.0], 420 mmol/L NaCl, 0.5% NP-40, 0.1 mmol/L EDTA, and 10% glycerol) for 45 minutes on ice. Samples were centrifuged at 13500*g* for 15 minutes, and the supernatant that contained chromatin-bound proteins was collected (chromatin fraction). The resultant pellet was resuspended in lysate buffer (above), sonicated for 10 seconds, and centrifuged at 1500*g* for 5 minutes at 4°C. The supernatant was collected (nuclear insoluble fraction).

Coimmunoprecipitation Assays

VSMCs were washed in PBS, harvested and lysed in 10% glycerol, 0.5 mmol/L EDTA, 25 mmol/L Tris-HCL (pH 7.5), 1 mmol/L Na_2VO_3, 180 mmol/L NaCl, 10 mmol/L β-glycerophosphate, 0.1 mmol/L DTT, and 0.1 % NP-40. Lysates were incubated with 4 µg anti-H2AX, rotating at 4°C, for 12 hours. Protein G agarose beads (Sigma) were then added to the lysates, washed 3× in lysis buffer, and boiled for 10 minutes before analysis by gel electrophoresis and Western blot (WB).

Boronate Bead Pull-Down Assay of PARylated Proteins

Beads coated in boronic acid resins bind to various oligonucleotides via vicinal diols. The chemical nature of PAR means PARylated proteins are a strong substrate for these beads and can be pulled down effectively in boronate bead pull-down assays (BBPDAs).[45] Six hours before BBPDAs, cells were treated with PARG (PAR glycohydrolase) inhibitor PDD00017273 (Sigma) to prevent PAR degradation, and any DNA damage treatments were performed. Nuclear fractions were collected as described in biochemical fractionation protocol, and this fraction was sonicated in lysate buffer (above) containing PARG inhibitor and mixed with m-aminophenylboronic acid agarose (No. A8312; Sigma) for 1 hour at room temperature. Following this incubation, beads were washed twice in SDS wash buffer (1% SDS, 100 mmol/L HEPES [pH 8.5], and 150 mmol/L NaCl) and twice in non-SDS wash buffer (100 mmol/L HEPES [pH 8.5] and 150 mmol/L NaCl). Proteins were eluted from beads by boiling for 10 minutes and analyzed by WB. For BBPDAs using protein from mouse aorta, vessels were homogenized in lysate buffer containing PARG inhibitor followed by sonication (3×10 seconds) and centrifugation at 2600*g* and 4°C for 5 minutes. Nine hundred fifty micrograms µg of protein was used in each reaction as described above.

Statistical Analysis

Results are presented as mean±SEM. Statistical analysis was performed with GraphPad software. All data were tested for normalcy using the Shapiro-Wilk test before comparison analysis. For comparisons of multiple groups, 1-way ANOVA with Tukey test was used. For comparison of just 2 independent

samples, the parametric Student *t* test was used. On graphs, **P*<0.05, ***P*<0.01, ****P*<0.001, *****P*<0.0001. Results were taken from a minimum of 3 independent experiments (technical replicates) using 3 different VSMC isolates (biological replicates). For histology, all groups were compared with the control group. The comparison was made using 1-way ANOVA test except for γH2AX where the Kruskal-Wallis test was used.

RESULTS

DNA Damage Augments VSMC Calcification in a Runx2-Dependent Manner

Primary human VSMCs cultured in calcifying media containing elevated Ca^{2+} and P_i exhibited visible signs of calcification after 5 days and were highly calcified after 15 days (Figure 1A; Figure IA in the Data Supplement). WB and immunofluorescence (IF) showed increased levels of the DNA damage marker γH2AX (Figure 1B and 1C; Figure IB through IG in the Data Supplement) in calcified VSMCs after 10 days of calcification treatment, and comet assays confirmed the presence of increased physical DNA damage in these cells (Figure 1D; Figure IH in the Data Supplement). Increased Runx2 protein levels (Figure 1B; Figure II in the Data Supplement) and concomitant loss of the smooth muscle marker SMA (smooth muscle actin) mirrored the induction of DNA damage and calcification.

To examine whether genomic stress could promote VSMC calcification, and whether this was dependent on Runx2, o-Cresolphthalein assays were performed on VSMCs cultured in control or calcifying media in the presence or absence of the DNA-damaging agents H_2O_2 (causes oxidative DNA damage) or etoposide (causes DNA double-strand breaks). In addition, levels of Runx2 were manipulated using adenoviral vectors (Figure IJ and IK in the Data Supplement). We found DNA damage alone did not induce VSMC calcification, but both agents augmented calcification when VSMCs were cultured in calcifying media (Figure 1E and 1F; Figure IL through IO in the Data Supplement). Knockdown of endogenous Runx2 via shRNA interference (shRunx2) had a minimal effect on reducing calcification induced by calcification media alone; however, the enhanced calcification caused by H_2O_2 or etoposide was completely abolished (Figure 1E and 1F). Conversely, adenovirus-mediated overexpression of FL-Runx2 increased calcification in calcifying media alone, and this increase was further enhanced with additional DNA damage caused by H_2O_2 or etoposide (Figure IL and IM in the Data Supplement). These data suggest that Runx2 is not essential for the initiation of VSMC calcification by elevated Ca^{2+} and P_i over this time course but Runx2 is pivotal in exacerbating calcification when genomic instability is high.

Increased calcification in response to genomic stress corresponded with enhanced transcription of Runx2 osteogenic targets. qRT-PCR (quantitative reverse transcription polymerase chain reaction) showed expression of *IBSP* (BSP), *Sp7* (Osterix), and *BGLAP* (OCN) was greatest in VSMCs grown in calcifying media supplemented with H_2O_2 with a small but significant increase in expression also seen in response to H_2O_2 treatment alone (Figure 1G through II). Runx2 depletion modestly suppressed expression of these genes in VSMCs cultured in calcifying media alone but more profoundly blocked the baseline and synergistic effects of H_2O_2. We also observed Runx2-dependent increased expression of *IBSP*, *Sp7*, and *BGLAP* in response to etoposide treatment (Figure IP through IR in the Data Supplement), showing Runx2 activity is also stimulated by DNA double-strand breaks. Additional putative Runx2 target genes *CDKN1A* (p21) and *MMP9* (matrix metalloproteinase 9; MMP9 protein) were also tested (Figure IS and IT in the Data Supplement), and although these genes increased expression in response to DNA damage and calcifying conditions, respectively, these changes were not dependent on Runx2. These data suggest that Runx2 osteogenic activity is most profound when genomic stress is applied to cells and that specific osteogenic targets may be preferentially expressed in response to genotoxic stress.

DNA Damage–Dependent Runx2 Accumulation, Osteogenic Gene Expression, and VSMC Calcification Are Reduced by PARP and ATM Inhibitors

To determine how Runx2 was influenced by genotoxic stress, VSMCs were exposed to either H_2O_2 or etoposide, and levels of Runx2 protein were quantified using WB (Figure 2A through 2C; Figure IIA through IIC in the Data Supplement) and IF (Figure IIC in the Data Supplement). These experiments revealed a significant increase in Runx2 protein levels following 3 hours of treatment that corresponded to increases in γH2AX. This was despite there being no change in Runx2 gene expression on qRT-PCR (Figure IID in the Data Supplement), suggesting a posttranscriptional mechanism was likely increasing Runx2 protein levels in response to DNA damage.

To identify potential signaling pathways that could posttranslationally elevate Runx2 protein following genotoxic stress, VSMCs were exposed to the same stressors but with the inclusion of inhibitors of DDR proteins PARP1/2 (PJ34) and ATM (Ku55933). These inhibitors were tested alongside inhibitors of ERK signaling (UO126), as this pathway has previously been implicated in VSMC calcification and Runx2 phosphorylation.[46,47] We observed that PARP and ATM inhibitors effectively blocked the increase in Runx2 protein in response to DNA damage; however, ERK inhibition did not (Figure 2D through 2F; Figure IIE through IIG in the Data Supplement).

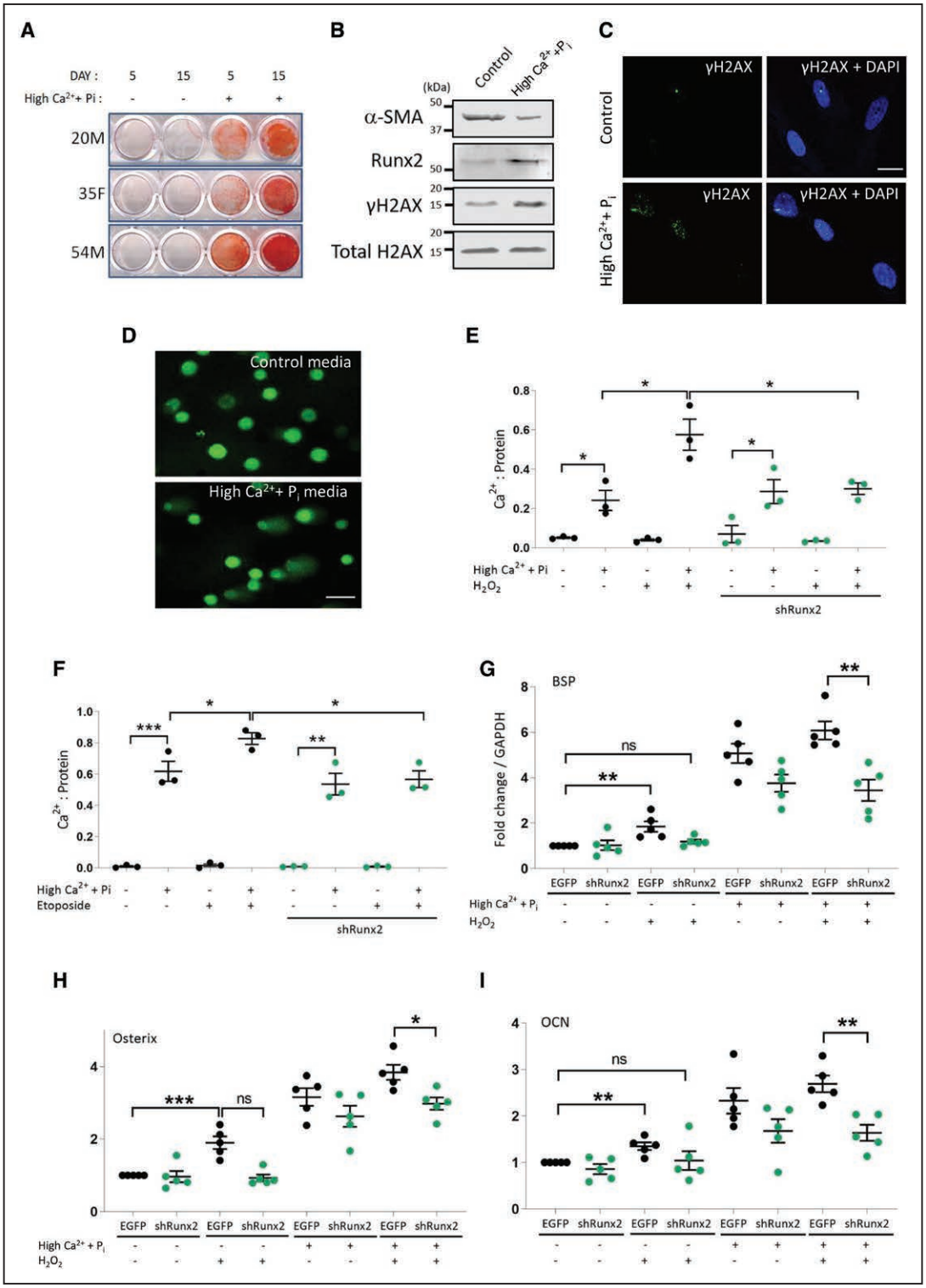

Figure 1. DNA damage augments vascular smooth muscle cell (VSMC) calcification in a Runx2 (Runt-related transcription factor 2)-dependent manner.

A, Alizarin red staining of 3 human VSMC isolates grown in control or calcifying media for 5 or 15 d. **B**, Western blot (WB) of protein lysate from VSMCs grown in control or calcifying media for 10 d (n=3; 35F isolate). **C**, Representative immunofluorescence of phosphorylation of histone H2AX on serine 139 (γH2AX) in 35F VSMCs grown in control or calcifying media (10 d), DAPI (4′,6-diamidino-2-phenylindole) is shown (blue), scale bar=20 μm. **D**, Representative comet assay, scale bar=40 μm. **E** and **F**, o-Cresolphthalein assay analysis showing calcification of 35F VSMCs depleted of Runx2 (shRunx2 [short hairpin RNA against Runx2]) and cultured in calcifying media, H_2O_2, etoposide, or combination treatment. Treatments were for 8 to 12 d (n=3). **G**–**I**, qRT-PCR (quantitative reverse transcription polymerase chain reaction) analysis of gene expression changes of Runx2 target genes *IBSP* (BSP [bone sialoprotein]), *Sp7* (Osterix), and *BGLAP* (OCN [osteocalcin]) in 35F VSMCs treated with EGFP (enhanced green fluorescent protein; control) or shRunx2 that were grown in control or calcifying media and with or without H_2O_2 treatment for 9 to 14 d. GAPDH was used as control gene (n=5). **P*<0.05, ***P*<0.01, ****P*<0.001. ns indicates not significant; and SMA, smooth muscle actin.

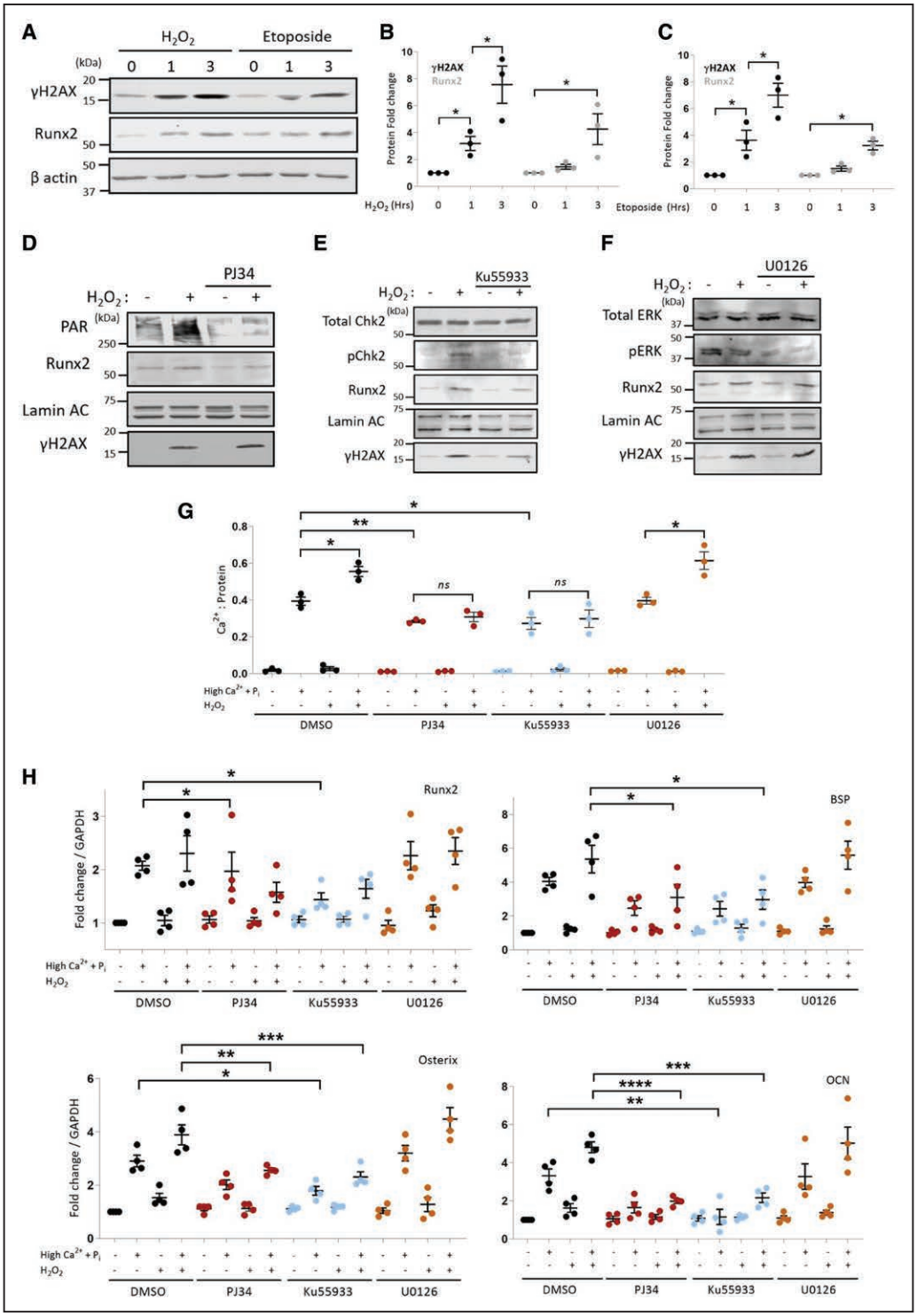

Figure 2. DNA damage–dependent Runx2 (Runt-related transcription factor 2) accumulation, vascular smooth muscle cell (VSMC) calcification, and osteogenic gene expression are reduced by PARP (poly[ADP-ribose] polymerase) and ATM (ataxia-telangiectasia mutated) inhibitors.

A, Western blot (WB) demonstrating Runx2 and phosphorylation of histone H2AX on serine 139 (γH2AX) increases in 35F VSMCs treated with H_2O_2 or etoposide. **B** and **C**, Quantification relative to β-actin (n=3). **D**–**F**, WBs showing PJ34 and Ku55933 suppress H_2O_2 (3-h treatment)-dependent Runx2 accumulation in 35F VSMCs but U0126 does not (n, minimum of 3). **G**, o-Cresolphthalein assay analysis showing 35F VSMC calcification following culture in calcifying media and H_2O_2 treatment (8–10 d) with additional PARP (PJ34), ATM (Ku55933), or ERK (extracellular signal-regulated kinase; U0126) inhibition (n=3). **H**, qRT-PCR (quantitative reverse transcription polymerase chain reaction) analysis investigating the effect of PARP, ATM, and ERK inhibition on *Runx2* (Runx2), *IBSP* (BSP [bone sialoprotein]), *Sp7* (Osterix), and *BGLAP* (OCN [osteocalcin]) gene expression in 35F VSMCs grown in control or calcifying media and treated with H_2O_2. Treatments were for 8 to 11 d. DMSO (dimethyl sulfoxide) was used as a negative control (n=3). **P*<0.05, ***P*<0.01, ****P*<0.001, *****P*<0.0001. Chk2 indicates checkpoint kinase 2; ns, not significant; PAR, poly(ADP-ribose); and pChk2, phospho-Chk2.

Consistent with the inhibitory effects of PJ34 and Ku55933 on Runx2 protein levels, these inhibitors also reduced VSMC calcification in response to calcifying media and completely blocked the augmented calcification induced by genotoxic stress (Figure 2G). Again, ERK inhibition had no effect. Reduced calcification also corresponded with reduced expression of Runx2 osteogenic target genes as evidenced by marked reductions in *IBSP*, *Sp7*, and *BGLAP* expression in VSMCs cultured in calcifying media, with the largest decrease seen in VSMCs cultured in calcifying media supplemented with H_2O_2 (Figure 2H).

DDR Causes Enhanced Runx2 Binding to Osteogenic Target Gene Promoters and Changes Its Nuclear Compartmentalization

We next assessed Runx2 occupancy at promoter regions of selected targets in VSMCs in response to genotoxic stress using chromatin immunoprecipitation assays and observed that Runx2 binding to osteogenic gene promoters *IBSP*, *Sp7*, and *BGLAP* was significantly increased by exposure to either H_2O_2 or etoposide (Figure 3A and 3B; Figure IIIA in the Data Supplement). However, Runx2 binding to its own promoter, *CDKN1A* or *MMP9* promoter regions, did not change with either treatment, consistent with the unresponsiveness of these genes to Runx2 depletion (Figure IS and IT in the Data Supplement). Both DDR inhibitors PJ34 and Ku55933 were effective at attenuating this increased binding (Figure 3C through 3E). The DNA repair factor Ku70 has been reported to regulate Runx2-mediated transactivation of some osteogenic targets,[48] but we saw no change upon Ku70 depletion (Figure IIIB and IIIC in the Data Supplement), suggesting it was not regulating increased Runx2 binding to osteogenic targets in response to genotoxic stress.

To further investigate how genomic stress influenced Runx2 compartmentalization, we used cell fractionation on VSMCs treated with H_2O_2 and observed that in response to oxidative stress, there was an increase in Runx2 specifically in the chromatin fraction (Figure 3F; Figure IIID in the Data Supplement). Treatment with PJ34 blocked this shift and resulted in retention of more Runx2 in the nuclear soluble fraction, showing that DNA damage affects Runx2 positioning within the nucleus and this is dependent on PARP signaling.

Runx2 Localizes to Sites of DNA Damage Induced by Both Etoposide and H_2O_2

The dynamic changes in compartmentalization in response to DNA damage led us to examine whether Runx2 may also play a functional role within the DDR. Using IF, we observed that both recombinant FL-Runx2 and endogenous Runx2 accumulated at sites of oxidative DNA damage caused by H_2O_2 and at DNA double-strand breaks induced by etoposide (Figure 4A through 4C; Figure IVA through IVH in the Data Supplement), with ≈40% of γH2AX associated with endogenous Runx2 foci.

Proper regulation and amplification of γH2AX is necessary for the integrity of the DDR and recruitment of repair factors. An important requirement for this is the dephosphorylation of an adjacent tyrosine 142 (pY142-H2AX) that in unstressed cells is constitutively phosphorylated.[49–51] Extensive DNA damage can result in retention of pY142-H2AX, which suppresses DNA repair pathways and results in apoptosis.[50,52] IF of Runx2 and pY142-H2AX revealed a degree of colocalization (Figure IVG in the Data Supplement). Further analysis using triple staining to visualize the spatial organization of Runx2 and pY142-H2AX together with γH2AX (Figure 4C; Figure IVH in the Data Supplement) showed that the Runx2/γH2AX complexes were arranged such that aggregations of Runx2 spatially separated H2AX histones presenting either the S139 or Y142 phosphorylated residues. Proximity ligation assays were used to further probe these arrangements and revealed that endogenous Runx2 interacted with both γH2AX and pY142-H2AX (Figure 4D; Figure IVI and IVJ in the Data Supplement) and that following genotoxic stress, significantly more Runx2/γH2AX interactions were detected (VSMCs with >15 observable interactions increased from ≈0%–70%) in conjunction with fewer Runx2/pY142-H2AX interactions (VSMCs with >15 observable interactions decreased from ≈65%–15%).

DNA Damage–Induced Runx2 Accumulation Promotes pY142-H2AX and Apoptosis

The close association between Runx2 and both γH2AX and pY142-H2AX led us to probe whether Runx2 influences either phosphorylated species. WB was used to test how depletion or overexpression of Runx2 affected γH2AX levels in VSMCs after H_2O_2 treatment (Figure 5A; Figure VA through VD in the Data Supplement). Compared with controls expressing EGFP, VSMCs treated with shRunx2 exhibited higher γH2AX at baseline and after H_2O_2 treatment. Conversely, overexpression of Runx2 (FL-Runx2) appeared to repress γH2AX, intimating that either these cells had less DNA damage or that γH2AX signaling had been attenuated and uncoupled from actual levels of DNA damage. To delineate this, comet assays were performed (Figure 5B; Figure VE in the Data Supplement), which demonstrated high levels of DNA damage in all samples treated with H_2O_2, supporting that elevated Runx2 protein acted to repress γH2AX. Moreover, both depletion and overexpression of Runx2 caused more DNA damage at baseline, inferring the DDR had become deregulated in both instances.

Next we explored how Runx2 might affect the relationship between γH2AX and pY142-H2AX as a potential mechanism that would account for uncoupling of the DDR and actual DNA damage. Using WB, we quantified how

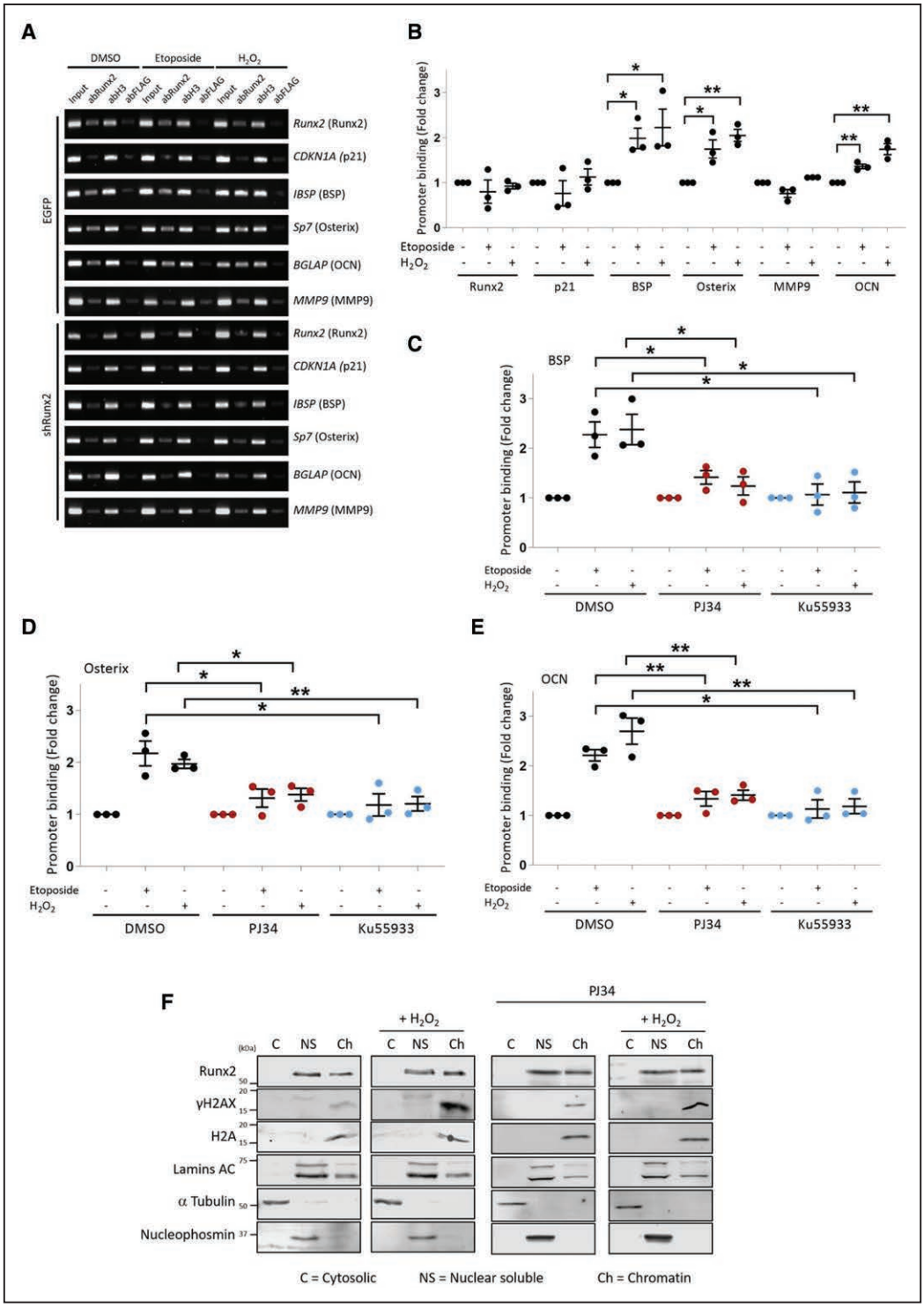

Figure 3. The DNA damage response causes enhanced Runx2 (Runt-related transcription factor 2) binding to osteogenic target gene promoters and changes in nuclear compartmentalization.

A, Polymerase chain reaction (PCR) analysis of Runx2 target promoter chromatin immunoprecipitation (ChIP) assays performed in control (EGFP [enhanced green fluorescent protein]) or shRunx2 (short hairpin RNA against Runx2)-treated 35F vascular smooth muscle cells (VSMCs) that were further treated with DMSO (dimethyl sulfoxide), etoposide, or H_2O_2 for 8 d. Anti-Runx2 (abRunx2; D130-3) was used to precipitate Runx2 and bound chromatin (Ch). abH3 was a positive control and abFLAG was a negative control. **B**, qPCR (quantitative PCR) analysis of Ch precipitated from control 35F VSMCs that were further treated with etoposide or H_2O_2 (5–8 d; n=3). **C**–**E**, qPCR analysis from ChIP assays investigating the effect of PARP (poly[ADP-ribose] polymerase; PJ34) and ATM (ataxia-telangiectasia mutated; Ku55933) inhibition on Runx2 binding to *IBSP* (BSP [bone sialoprotein]), *Sp7* (Osterix), and *BGLAP* (OCN [osteocalcin]) promoter regions in 35F VSMCs treated with etoposide or H_2O_2 for 5 to 10 d. DMSO was used as an NO inhibitor control (n=3). **F**, Western blot of biochemical fractionation of 35F VSMCs following 3-h H_2O_2 treatment with or without PJ34. Cells were fractioned into cytosolic (C), nuclear soluble (NS), and Ch fractions. **P*<0.05, ***P*<0.01. MMP9 indicates matrix metalloproteinase 9.

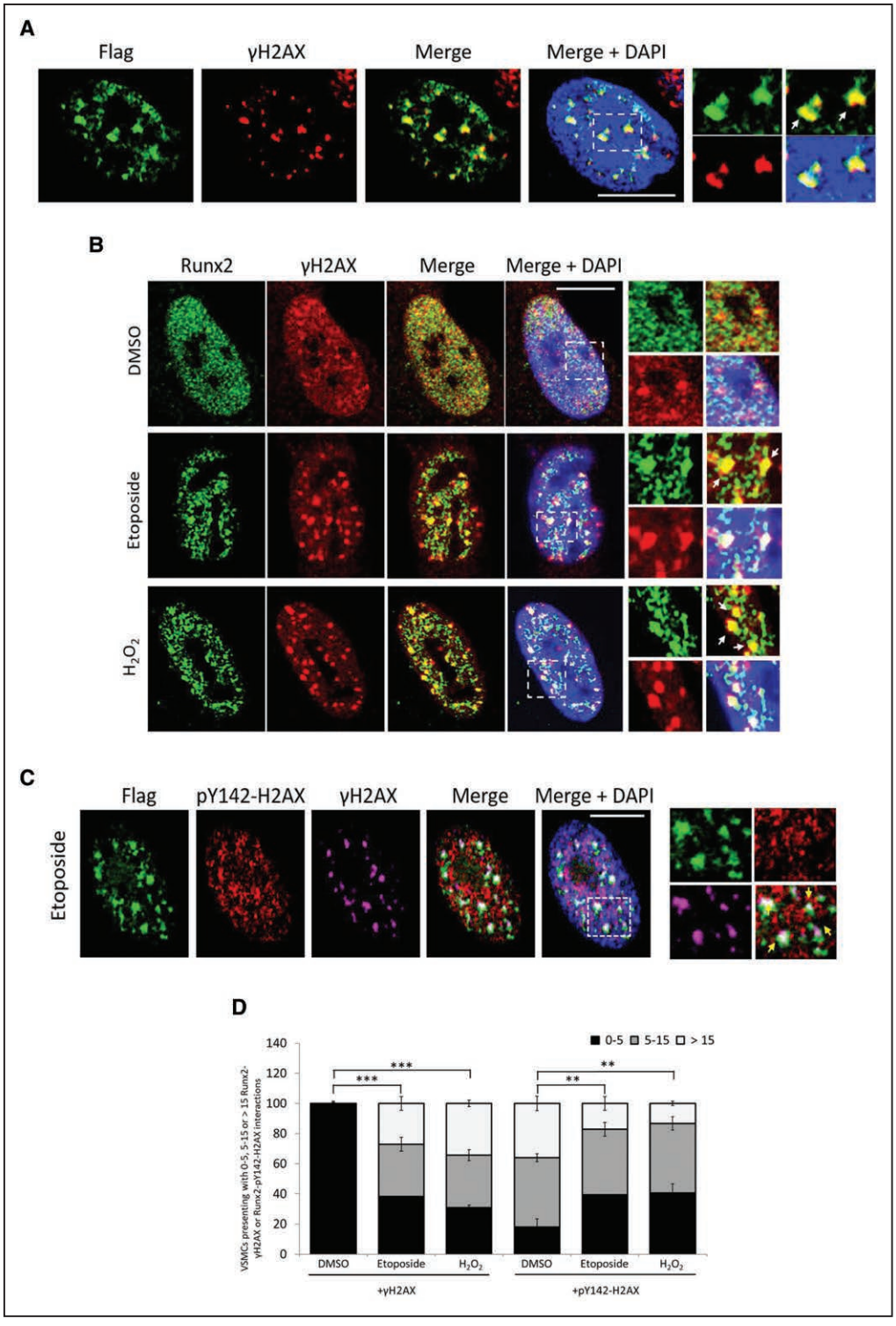

Figure 4. Runx2 (Runt-related transcription factor 2) forms distinct nucleoplasmic structures that are spatially associated with phosphorylation of histone H2AX on serine 139 (γH2AX) and phosphorylated tyrosine 142 on H2AX (pY142-H2AX).
A, Immunofluorescence (IF) showing FL-Runx2 (recombinant FLAG-tag Runx2; Flag) and γH2AX in 35F vascular smooth muscle cells (VSMCs) treated with H_2O_2 (3 h). White arrows indicate colocalization. DNA is stained with DAPI (4′,6-diamidino-2-phenylindole; blue). Scale bar=10 μm. **B**, IF showing endogenous Runx2 and γH2AX in 35F VSMCs treated with DMSO (dimethyl sulfoxide), etoposide, or H_2O_2 (3 h). DNA is stained with DAPI (blue). White arrows indicate colocalization. Scale bar=10 μm. **C**, Triple staining IF image showing FL-Runx2, pY142-H2AX, and γH2AX in a 35F VSMC treated with etoposide (3 h). DNA is stained with DAPI (blue). Yellow arrows indicate colocalization of FL-Runx2 and γH2AX in pockets devoid of pY142-H2AX. Scale bar=10 μm. **D**, Quantification of proximity ligation assays (means from 3 independent experiments with n>100 cells per experiment) is also shown. Cells were grouped into 0 to 5 (low genomic damage), 5 to 15 (moderate genomic damage), and >15 foci (high genomic damage)/cell groups. Comparisons were performed on >15 groups. ***P*<0.01, ****P*<0.001.

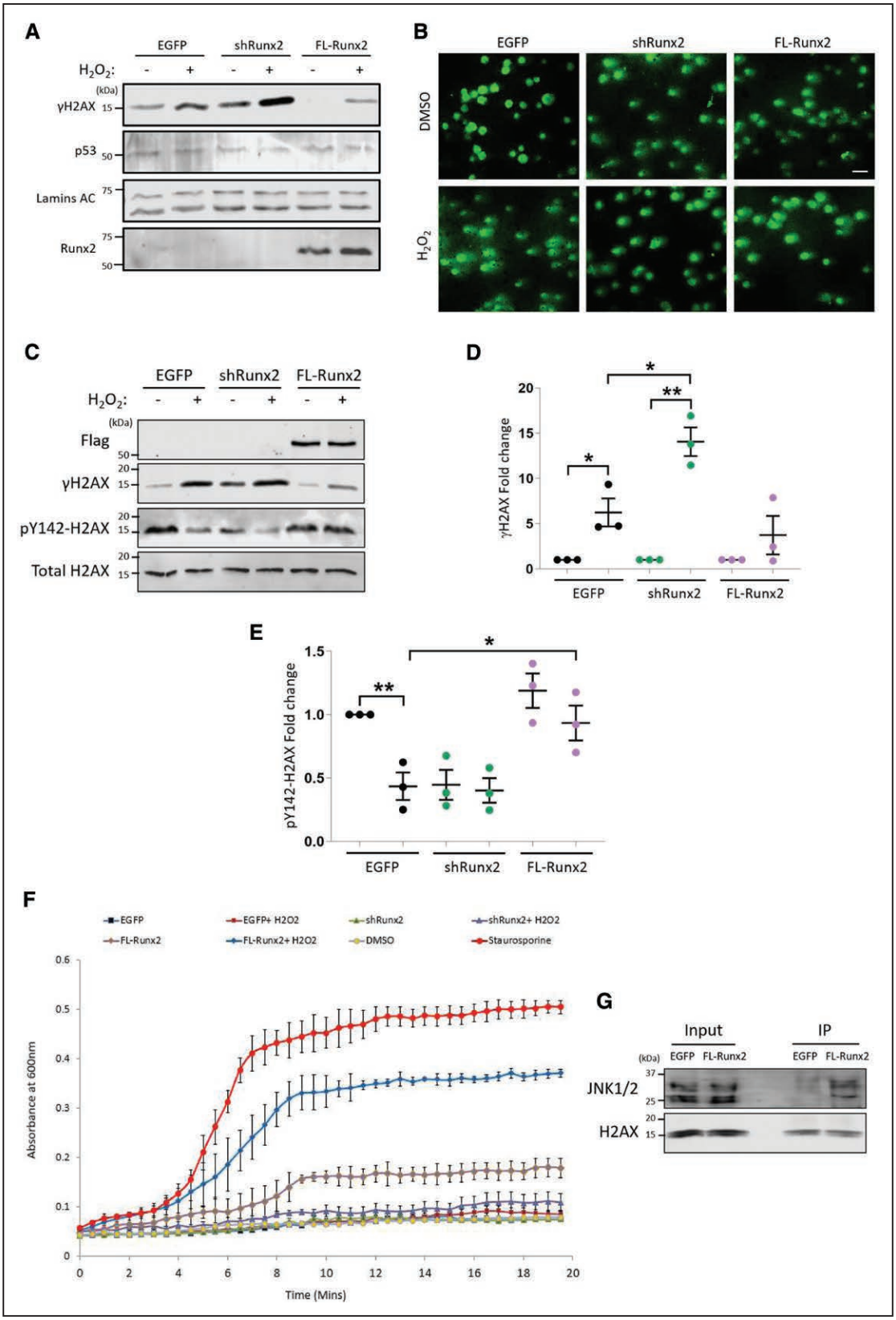

Figure 5. Runx2 (Runt-related transcription factor 2) represses phosphorylation of histone H2AX on serine 139 (γH2AX) following genotoxic stress and promotes retention of phosphorylated tyrosine 142 on H2AX (pY142-H2AX) causing increased vascular smooth muscle cell (VSMC) apoptosis.

A, Western blot (WB) showing dysregulated γH2AX caused by Runx2 overexpression or depletion in 35F VSMCs at both baseline and after H_2O_2 (3-h treatment). Lamins AC and p53 were unaffected by Runx2. **B**, Representative comet assay raw data (*Continued*)

both modifications changed in human VSMCs in response to H_2O_2 treatment and observed that upon application of stress, a reduction in pY142-H2AX occurred concurrently with γH2AX accrual (Figure VF through VH in the Data Supplement). We then investigated how Runx2 influenced this switch and observed that VSMCs expressing FL-Runx2 retained more pY142-H2AX after H_2O_2 (Figure 5C through 5E; Figure VI in the Data Supplement). Conversely, depletion of Runx2 resulted in less pY142-H2AX in both stressed and unstressed conditions. Analysis of γH2AX and pY142-H2AX levels in primary VSMCs derived from smooth muscle–specific Runx2 KO mice revealed similar findings, with unstressed cells presenting with higher γH2AX and lower pY142-H2AX compared with controls and markedly higher γH2AX following H_2O_2 (Figure VJ through VM in the Data Supplement).

The above data supported a mechanism whereby high levels of Runx2 favored pY142-H2AX and repressed γH2AX even when DNA damage was present. As this configuration is associated with apoptosis via JNK (c-Jun N-terminal protein kinase) signaling,[50] we used an active caspase-3 assay to assess levels of apoptosis and found overexpression of Runx2 led to increased levels of CC3 (Figure 5F; Figure VN in the Data Supplement). These levels were amplified further when H_2O_2 was present. Coimmunoprecipitation assays showed that overexpression of Runx2 increased the amount of JNK proteins interacting with H2AX (Figure 5G; Figure VO in the Data Supplement) under genomic stress, which would be anticipated if Runx2 promotes apoptosis via repression of the DDR and subsequent recruitment of JNK.[52]

Runx2 Is PARylated in Response to Genotoxic Stress, and PARP Inhibitors Block Its Localization at Sites of DNA Damage

The marked effect of DDR inhibitors upon Runx2 activity led us to test whether localization of Runx2 at sites of DNA damage was affected when DDR signaling was impaired. As ATM inhibitors would directly suppress γH2AX phosphorylation, we focused on the effect of PARP inhibition. To mitigate the anticipated lower levels of Runx2 following PARP inhibition under genotoxic stress, we investigated interactions between γH2AX and overexpressed FL-Runx2. We identified significantly fewer cells that contained ≥15 interactions between γH2AX and FL-Runx2 after etoposide treatment in cells treated with PJ34 (Figure 6A), implying PARP activity is involved in Runx2 localization to sites of DNA damage.

Recent evidence has emerged that PARylation of Runx3 is necessary for its involvement in repair of cross-links in DNA.[53] The two sites within the Runx3 protein that were previously identified as being subject to PARylation[54] are conserved within Runx2 (Figure 6B), leading us to test whether PARylation of Runx2 was responsible for its increased stability in response to DNA damage. For this, BBPDAs using beads that attach to covalently bound PARylated residues[45] were performed. These experiments showed that significantly more endogenous Runx2 was pulled down from VSMCs cultured in calcifying media, H_2O_2, or etoposide compared with controls (Figure 6C; Figure VIA in the Data Supplement) and that PJ34 abolished this increase in all instances. As late passage presenescent VSMCs exhibit more DNA damage and endogenous Runx2 accumulation, as well as osteogenic differentiation,[33] we also tested whether there was more PARylated Runx2 in these cells, and BBPDAs confirmed this was the case (Figure VIB and VIC in the Data Supplement).

To further confirm that genomic stress directly induced PARylation of Runx2, we repeated BBPDAs in VSMCs expressing FL-Runx2. This allayed the possibility that the higher incidence of endogenous PARylated Runx2 pull-down that was observed was caused by differences in total Runx2 protein levels resulting from different treatments. As the total input of FL-Runx2 was the same in stressed or nonstressed cells, any increase in Runx2 pull-down would be evidence of Runx2 PARylation. As shown in Figure 6D and 6E and Figure VID and VIE in the Data Supplement, induction of DNA damage by H_2O_2 or etoposide resulted in increased PARylated Runx2, and this was abolished in the presence of the PARP inhibitor PJ34. Inhibition of ATM also lowered levels of PARylated FL-Runx2 after genotoxic stress (Figure 6F; Figure VIF in the Data Supplement), suggesting ATM activity is upstream of this modification.

Runx2 Localizes With γH2AX in Calcified Arteries and Is Essential for Osteogenic Gene Expression In Vivo

To analyze the relationship between Runx2 and DNA damage during calcification in vivo, immunohistochemistry

Figure 5 Continued. showing 35F VSMCs expressing either EGFP (enhanced green fluorescent protein; control), FL-Runx2 (recombinant FLAG-tag Runx2), or shRunx2 (short hairpin RNA against Runx2) and treated for 3 h with DMSO (dimethyl sulfoxide) or H_2O_2. DNA is stained with Nancy-520. Scale bar=40 μm. **C**, WB of γH2AX and pY142-H2AX in 35F VSMCs expressing EGFP, shRunx2, or FL-Runx2 and treated with H2O2 for 3 hours. Total H2AX is shown as a control. **D**, Quantification of band intensities of γH2AX from experiments shown in **C**. **E**, WB of γH2AX and pY142-H2AX in 35F VSMCs expressing EGFP, shRunx2, or FL-Runx2 and treated with H_2O_2 for 3 h. Total H2AX is shown as a control. **F** and **G**, Quantification of band intensities of both γH2AX and pY142-H2AX from experiments shown in **E** (n=3). **F**, Data from active caspase 3 ELISA. 35F VSMCs expressing EGFP, shRunx2, or FL-Runx2 were treated for 3 h with H_2O_2 to determine sensitivity to apoptosis. Absorbance at 600 nm represents levels of cleaved caspase-3. Staurosporine was used as a positive control for apoptosis (n=3). **G**, WB of coimmunoprecipitation assay investigating JNK (c-Jun N-terminal protein kinase) binding to H2AX. 35F VSMCs expressing either EGFP or FL-Runx2 were treated for 3 h with etoposide before using H2AX as bait to pull-down JNK. The two bands represent JNK1 and 2. *P<0.05, **P<0.01. IP indicates immunoprecipitation.

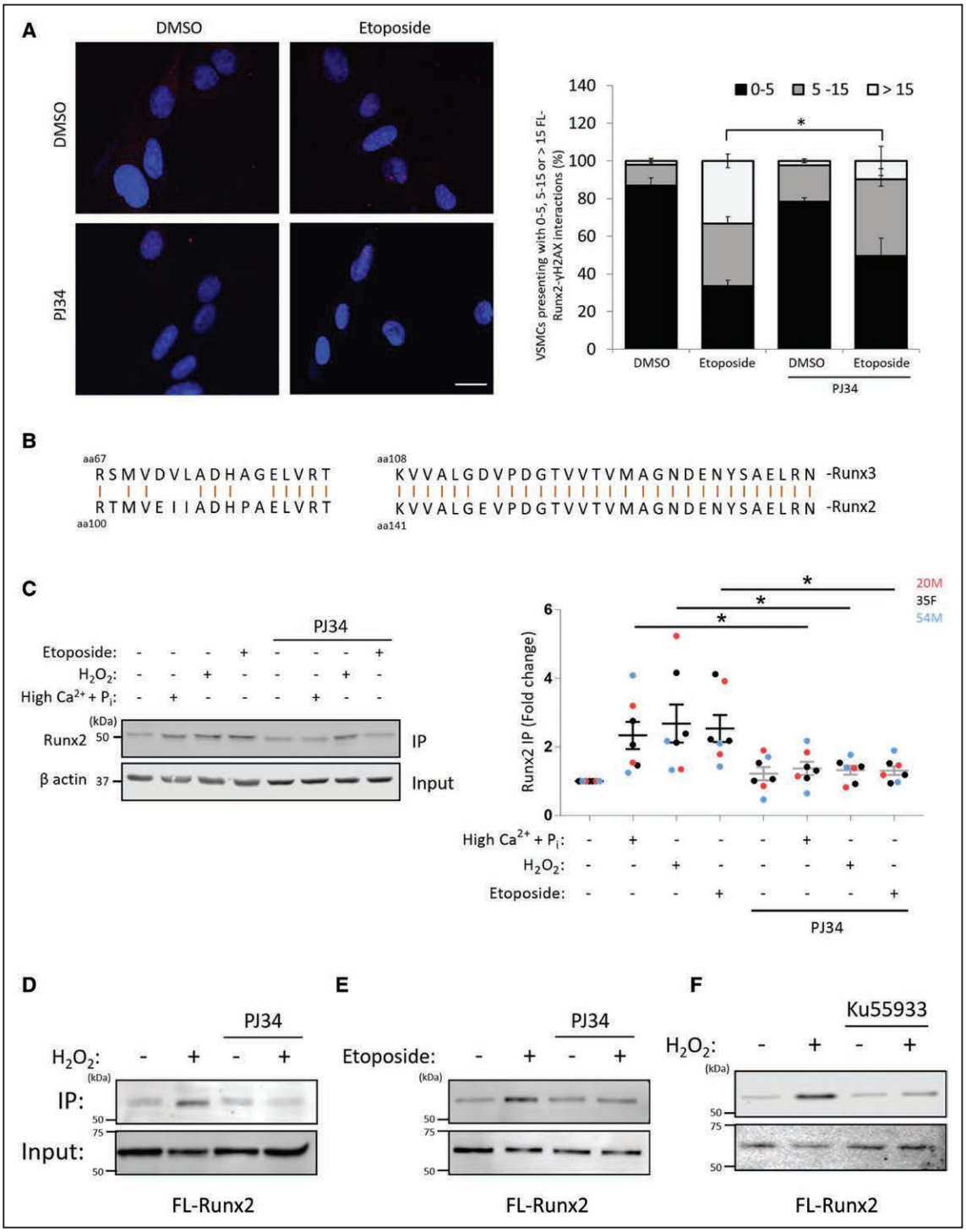

Figure 6. Runx2 (Runt-related transcription factor 2) is PARylated in response to genotoxic stress.
A, Representative image and quantification of PLAs investigating FL-Runx2 (recombinant FLAG-tag Runx2) interactions with phosphorylation of histone H2AX on serine 139 in 35F vascular smooth muscle cells (VSMCs) treated for 3 h with etoposide and additional PJ34 treatment (means from 3 independent experiments with n>100 cells). Scale bar=20 µm. Cells were grouped into 0 to 5 (low genomic damage), 5 to 15 (moderate genomic damage), and >15 foci (high genomic damage)/cell groups. Comparisons were performed on >15 groups. **B**, Amino acid sequence analysis showing hypothesized PARylated regions within Runx3 are conversed within Runx2. **C**, Western blot (WB) and quantification from boronate bead pull-down assays (BBPDAs) of endogenous Runx2 from 3 VSMCs isolates treated with calcifying media, H_2O_2 or etoposide for 11 to 14 d. PJ34 treatment was used to assess PARP (poly[ADP-ribose] polymerase) inhibition. β-actin shows lysate input. For quantification, fold change of Runx2 was normalized to β-actin input (n=7). **D**, WB from BBPDAs of FL-Runx2 expressed in 35F VSMCs treated with or without H_2O_2 and PJ34 PARP inhibitor (3-h treatments; n=4). **E**, WB from BBPDAs of FL-Runx2 expressed in 35F VSMCs treated with or without etoposide and PJ34 PARP inhibitor (3-h treatments; n=5). **F**, Representative WB from BBPDAs of FL-Runx2 expressed in 35F VSMCs treated with or without H_2O_2 and Ku55933 ATM (ataxia-telangiectasia mutated) inhibitor (3-h treatments; n=4). *P<0.05. IP indicates immunoprecipitation.

was performed on the aorta of rats using a model where calcification is induced by dysregulated mineral metabolism caused by chronic renal failure. Calcification occurred at week 4 after induction, and at this time point, levels of DNA damage, shown by increased γH2AX and 8-oxodG staining, peaked, as did the accumulation of nuclear Runx2 (Figure VIIA in the Data Supplement). Moreover, VSMCs positive for these markers were in close proximity to calcified regions. At week 8, there was a reduction in cells positive for Runx2 and DNA damage markers, which may be explained by apoptosis of Runx2-positive VSMCs at sites of calcification.

To examine this further in a more dynamic model of vascular calcification, wild-type (*Runx2*$^{f/f}$) and smooth muscle–specific *Runx2* KO mice (*Runx2*$^{\Delta SM}$) were treated with VitD to induce mineral dysregulation and aortic calcification. As anticipated, VitD treatment increased levels of Runx2 in the aorta of *Runx2*$^{f/f}$ mice, but this was greatly attenuated in *Runx2*$^{\Delta SM}$ mice (Figure 7A; Figure VIIB in the Data Supplement). Using immunohistochemistry, we found that VitD treatment induced elevated levels of DNA damage as shown by increased γH2AX staining in the aorta of both *Runx2*$^{f/f}$ and *Runx2*$^{\Delta SM}$ (Figure 7B; Figure VIID in the Data Supplement); however, we were unable to detect significant alterations in pY142-H2AX as levels were highly variable (data not shown).

Runx2$^{\Delta SM}$ mice were resistant to calcification as shown by the absence of von Kossa–positive staining in the aorta after VitD treatment (Figure 7B) and also reduced calcium accumulation in o-Cresolphthalein assays (Figure VIIC in the Data Supplement). Consistent with Runx2 driving apoptosis in response to higher levels of DNA damage, quantification of CC3 (which gives a snapshot of apoptosis) showed that VitD caused a significant increase in apoptotic cells in *Runx2*$^{f/f}$ animals but not in *Runx2*$^{\Delta SM}$ mice (Figure VIIE in the Data Supplement). Conversely, TUNEL staining revealed high staining in *Runx2*$^{\Delta SM}$ mice after VitD treatment (Figure VIIF in the Data Supplement) most likely indicative of DNA breaks, which is consistent with sustained and elevated DNA damage due to destabilization of the DDR[55] in *Runx2*$^{\Delta SM}$ mice.

qRT-PCR for Runx2 and its targets in mice with or without VitD treatment showed Runx2 expression was low in *Runx2*$^{\Delta SM}$ mice and modestly increased in *Runx2*$^{f/f}$ mice in response to VitD. Increased expression of Runx2 targets including *Runx2* itself, *IBSP*, *Sp7*, and *BGLAP* was induced in control animals in response to VitD but not in *Runx2*$^{\Delta SM}$ mice (Figure 7C through 7F). However, as seen during in vitro studies, other Runx2 targets *CDKN1A* and *MMP9* showed no difference in expression between *Runx2*$^{f/f}$ or *Runx2*$^{\Delta SM}$ mice (Figure VIIG in the Data Supplement). To ascertain whether increased osteogenic differentiation was associated with increased PARylation of Runx2, BBPDAs were again used (Figure 7G). These showed higher levels of PARylated Runx2 in VitD-treated *Runx2*$^{f/f}$ mice that were not observed in *Runx2*$^{\Delta SM}$ mice, supporting the notion that genomic stress–induced PARylation of Runx2 leads to activation of a subset of specific osteogenic targets to enhance calcification.

DISCUSSION

Runx2 in the DDR and Biomineralization

This study has delineated how Runx2 governs VSMC phenotype in response to genomic stress and identifies ATM and PARP signaling as key drivers of calcification. Runx2 was identified as a component of the DDR where it localized to sites of DNA damage where its role in regulating H2AX phosphorylation events was tightly coupled to VSMC osteogenic reprogramming and JNK-mediated apoptosis. Previous studies have robustly demonstrated that a combination of VSMC phenotypic switching and apoptosis work in concert to drive calcification,[14,56] but this study stands alone in implicating Runx2 in driving both these processes with these activities dependent on activation of the DDR.

Runx2 Regulates the DDR and Couples It to Transcriptional Reprogramming

In vitro, agents that caused genotoxic stress accelerated VSMC calcification, and this correlated with Runx2 accumulation and increased osteogenic activity, both of which were blocked by DDR inhibitors. Similarly in vivo, calcification induced by dysregulated mineral metabolism due to CKD or VitD overload was associated with DNA damage and Runx2 accumulation at calcified sites. This was temporally associated with activation of osteogenic genes and apoptosis. In the absence of Runx2, osteogenic differentiation, apoptosis, and calcification were ameliorated.

The accumulation of Runx2 in response to genotoxic stress correlated with its PARylation both in vitro and in vivo in calcified arteries. In vitro studies showed that this modification was required for its localization to sites of DNA damage, increased promoter occupancy, and activation of specific osteogenic targets. Inhibition of the DDR using either ATM or PARP inhibition blocked Runx2 localization to sites of DNA damage, osteogenic responses, and calcification.

Genomic stress led to increased chromatin association of Runx2 and specific activation of osteogenic targets; however, the mechanisms linking Runx2 function in the DDR with osteogenic cell fate are unknown. We ruled out a role for the DDR-dependent transcriptional cofactor Ku70[48] although it is possible that other Runx2-binding partners may regulate target specificity.[57] Another plausible explanation could be linked to its association with the nuclear

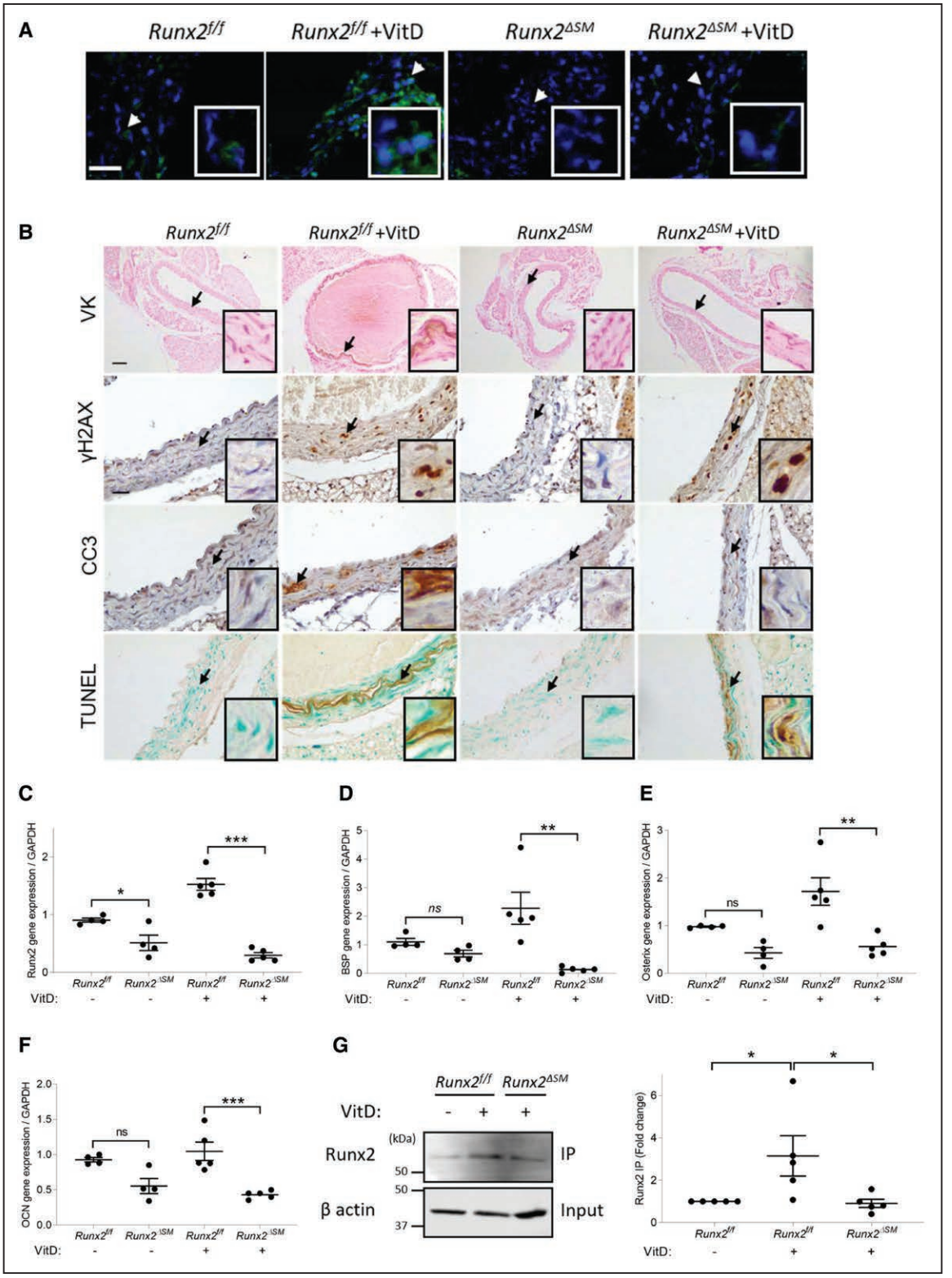

Figure 7. Runx2 (Runt-related transcription factor 2) localizes with phosphorylation of histone H2AX on serine 139 (γH2AX) in calcified arteries, is essential for osteogenic gene expression, and is PARylated in response to vitamin D (VitD) treatment in vivo. **A**, Immunofluorescence of Runx2 staining (green) in control (*Runx2*$^{f/f}$) and smooth muscle–specific Runx2 knockout (*Runx2*$^{\Delta SM}$) mice aortas treated with or without VitD. White arrows show enlarged area, scale bar=30 μm. **B**, Immunohistochemistry of aorta from the same mice stained for von Kossa (calcified regions), γH2AX (DNA damage), CC3 (cleaved caspase-3 [apoptosis]), and TUNEL (terminal deoxynucleotidyl transferase dUTP nick-end labeling) staining (fragmented DNA [**C–F**] qRT-PCR [quantitative reverse transcription polymerase chain reaction] of *Runx2* [Runx2], *IBSP* [BSP (bone sialoprotein)], *Sp7* [Osterix], and *BGLAP* [OCN (osteocalcin)] in *Runx2*$^{f/f}$ and *Runx2*$^{\Delta SM}$ mice aorta treated with or without VitD [n=5]). **G**, Boronate bead pull-down assay data showing PARylation of Runx2 in *Runx2*$^{f/f}$ and *Runx2*$^{\Delta SM}$ mice aorta. Representative Western blot (**left**) and quantification (**right**) is shown (n=5). **P*<0.05, ***P*<0.01, ****P*<0.001. IP indicates immunoprecipitation; ns, not significant; and VK, von Kossa stain.

matrix. This scaffold can regulate chromatin organization and histone modifications,[58,59] which are important for both transcription and the DDR. Previous studies have shown that Runx2 can recruit chromatin-modifying proteins including BAZ1B (bromodomain adjacent to zinc finger domain, 1B) protein to sites of DNA damage in cancer cells.[24] In addition, Runx2 can regulate expression of a number of epigenetic modifiers including EZH2 (enhancer of zeste homolog 2)[60] that modulate gene expression at multiple sites across the genome. A combination of these functions might allow global epigenetic modifications to drive changes in gene expression in response to DNA damage. Further analysis of Runx2 targets in VSMCs is required to confirm these mechanisms and target specificity.

Runx2, DDR Signaling, and Apoptosis

Until now, understanding of the involvement of Runx2 in the DDR has been limited.[24,29,61,62] Conversely, more precise functions for Runx1 and 3 have been documented. Both are PARylated in response to genome damage[53,63] and bind to DNA repair structures. Runx3 has a recognized role in DNA cross-link repair and interacts with the RecQ helicase Bloom syndrome helicase to recruit FANCD2 (Fanconi anemia complementation group D2),[53] with this function being blocked by PARP inhibitors. We observed that Runx2 is also PARylated following DNA damage, and this was necessary for its localization to DNA repair sites. Here, it led to retention of pY142-H2AX and suppression of γH2AX levels even after DNA damage induction. The cophosphorylation of both γH2AX and pY142-H2AX is associated with DNA repair repression and initiation of apoptosis through recruitment of the proapoptotic factor JNK to H2AX.[50] It is thought that duel phosphorylation of both residues prevents binding of key DNA repair scaffold protein MDC1 (mediator of DNA damage checkpoint protein 1)[64] and inhibition of DNA repair. In this scenario, unrepaired DNA damage will accumulate, and this stimulates JNK translocation into the nucleus and subsequent phosphorylation of substrates involved in caspase-activated DNase degradation of DNA, including H2AX.[65] This process is mediated by PTB-domain protein Fe65, which binds to pY142-H2AX under conditions of stress and recruits JNK.[50] How Runx2 promotes pY142-H2AX under genotoxic stress conditions and induces this apoptotic pathway remains to be elucidated; however, it would be important to investigate whether Runx2 influences the activities of the phosphatase Eya (eyes absent)[50] or WSTF (Williams syndrome transcription factor) kinase,[49] both of which determine Y142-H2AX phosphorylation. Our data suggested that elevated levels of Runx2 were required to drive this apoptotic process suggesting that chronically elevated genotoxic stress, as observed in aging and disease, might be requisite to induce this activity.

While the precise cue that dictates whether Runx2 favors VSMC osteogenic transition or induction of apoptosis is not certain, we propose that the amount and persistence of DNA damage is likely an important factor, with more and prolonged damage favoring cell death (Figure VIII in the Data Supplement). Interestingly, JNK-mediated apoptosis has been documented to be associated with development,[66] so whether proapoptotic activity of Runx2 is also present in the bone growth plate, where γH2AX-positive cells have been recorded,[35] would be important to investigate as this would suggest that the coupling of DNA damage, osteogenic transcription, and apoptosis via Runx2 are also key to bone development.

DDR as a Therapeutic Target for Calcification

In this study, we have underlined a key role for the activation of Runx2 by genomic stress during vascular biomineralization. We observed that arresting DDR signaling via either ATM or PARP inhibition blocked DNA damage–dependent Runx2 PARylation and VSMC calcification, and our data support a model whereby ATM activity is upstream of the PARPs responsible for PARylation of Runx2. Previous studies have shown synergistic activity of these enzymes, in the case of recruitment of Kif2C (kinesin family member 2C) to DNA damage[67] and also in the formation of ATM and PARP1 complexes that influence cross talk between DDR signaling pathways.[68] Although further work is required to determine how these pathways might intersect during VSMC calcification and regulate Runx2 activity, our data do highlight the potential of inhibitors of the DDR as therapeutics for vascular calcification. In addition, we speculate that DDR activation of Runx2 may also be important in a number of other contexts where DNA damage and senescence have been linked to ectopic calcification including atherosclerosis,[35] diabetic vasculopathy,[69] age- and radiation-induced aortic stenosis,[70] as well as senescence-associated mineralization of skeletal muscle[71] and connective tissues.[22,23] We also speculate that activation of Runx2 by the DDR may be important for normal bone formation, but further exploration into these possibilities is now required. Taken together, our data indicate that Runx2 exhibits characteristics of an antagonistic pleiotropic gene, with its important role during bone development outweighing a detrimental function as a promoter of ectopic mineralization.

ARTICLE INFORMATION

Received August 25, 2020; accepted December 8, 2020.

Affiliations

BHF Centre of Research Excellence, School of Cardiovascular Medicine and Sciences, King's College London, The James Black Centre, United Kingdom (A.M.C., S.Y., R.H., S.A., M.S., C.M.S.). Laboratory of Pathophysiology, Department of Biomedical Sciences, University of Antwerp, Wilrijk, Belgium (A.V., P.C.D.).

Acknowledgments

We thank the Wohl Cellular Imaging Centre at King's College London for help with light microscopy. A.M. Cobb and C.M. Shanahan contributed to the conceptualization; A.M. Cobb, R. Hayward, A. Verhulst, P.C. D'Haese, and C.M. Shanahan

to methodology; A.M. Cobb, R. Hayward, and S. Ahmad to formal analysis; A.M. Cobb, R. Hayward, and S. Ahmad to investigation; R. Hayward, M. Sun, A. Verhulst, P.C. D'Haese, and C.M. Shanahan to Resources; A.M. Cobb and C.M. Shanahan to writing the original draft; A.M. Cobb, S. Yusoff, R. Hayward, S. Ahmad, M. Sun, A. Verhulst, P.C. D'Haese, and C.M. Shanahan to writing review and editing; C.M. Shanahan to supervision; C.M. Shanahan to project administration; and C.M. Shanahan and P.C. D'Haese to funding acquisition.

Sources of Funding

Work by A.M. Cobb, S. Ahmad, S. Yusoff, R. Hayward, and M. Sun was supported by a British Heart Foundation Programme Grant to C.M. Shanahan (RG/17/2/32808). A. Verhulst and P.C. D'Haese were funded by the University of Antwerp.

Disclosures

None.

REFERENCES

1. Nicoll R, Henein MY. The predictive value of arterial and valvular calcification for mortality and cardiovascular events. *Int J Cardiol Heart Vessel.* 2014;3:1–5. doi: 10.1016/j.ijchv.2014.02.001
2. Wayhs R, Zelinger A, Raggi P. High coronary artery calcium scores pose an extremely elevated risk for hard events. *J Am Coll Cardiol.* 2002;39:225–230. doi: 10.1016/s0735-1097(01)01737-5
3. Aladin AI, Al Rifai M, Rasool SH, Dardari Z, Yeboah J, Nasir K, Budoff MJ, Psaty BM, Blumenthal RS, Blaha MJ, et al. Relation of coronary artery calcium and extra-coronary aortic calcium to incident hypertension (from the Multi-Ethnic Study of Atherosclerosis). *Am J Cardiol.* 2018;121:210–216. doi: 10.1016/j.amjcard.2017.10.018
4. Kapustin AN, Chatrou ML, Drozdov I, Zheng Y, Davidson SM, Soong D, Furmanik M, Sanchis P, De Rosales RT, Alvarez-Hernandez D, et al. Vascular smooth muscle cell calcification is mediated by regulated exosome secretion. *Circ Res.* 2015;116:1312–1323. doi: 10.1161/CIRCRESAHA.116.305012
5. Durham AL, Speer MY, Scatena M, Giachelli CM, Shanahan CM. Role of smooth muscle cells in vascular calcification: implications in atherosclerosis and arterial stiffness. *Cardiovasc Res.* 2018;114:590–600. doi: 10.1093/cvr/cvy010
6. Steitz SA, Speer MY, Curinga G, Yang HY, Haynes P, Aebersold R, Schinke T, Karsenty G, Giachelli CM. Smooth muscle cell phenotypic transition associated with calcification: upregulation of Cbfa1 and downregulation of smooth muscle lineage markers. *Circ Res.* 2001;89:1147–1154. doi: 10.1161/hh2401.101070
7. Ozaki T, Yu M, Yin D, Sun D, Zhu Y, Bu Y, Sang M. Impact of RUNX2 on drug-resistant human pancreatic cancer cells with p53 mutations. *BMC Cancer.* 2018;18:309. doi: 10.1186/s12885-018-4217-9
8. Javed A, Gutierrez S, Montecino M, van Wijnen AJ, Stein JL, Stein GS, Lian JB. Multiple Cbfa/AML sites in the rat osteocalcin promoter are required for basal and vitamin D-responsive transcription and contribute to chromatin organization. *Mol Cell Biol.* 1999;19:7491–7500. doi: 10.1128/mcb.19.11.7491
9. Ducy P, Zhang R, Geoffroy V, Ridall AL, Karsenty G. Osf2/Cbfa1: a transcriptional activator of osteoblast differentiation. *Cell.* 1997;89:747–754. doi: 10.1016/s0092-8674(00)80257-3
10. Shanahan CM, Cary NR, Salisbury JR, Proudfoot D, Weissberg PL, Edmonds ME. Medial localization of mineralization-regulating proteins in association with Mönckeberg's sclerosis: evidence for smooth muscle cell-mediated vascular calcification. *Circulation.* 1999;100:2168–2176. doi: 10.1161/01.cir.100.21.2168
11. Tyson KL, Reynolds JL, McNair R, Zhang Q, Weissberg PL, Shanahan CM. Osteo/chondrocytic transcription factors and their target genes exhibit distinct patterns of expression in human arterial calcification. *Arterioscler Thromb Vasc Biol.* 2003;23:489–494. doi: 10.1161/01.ATV.0000059406.92165.31
12. Kapustin AN, Schoppet M, Schurgers LJ, Reynolds JL, McNair R, Heiss A, Jahnen-Dechent W, Hackeng TM, Schlieper G, Harrison P, et al. Prothrombin loading of vascular smooth muscle cell-derived exosomes regulates coagulation and calcification. *Arterioscler Thromb Vasc Biol.* 2017;37:e22–e32. doi: 10.1161/ATVBAHA.116.308886
13. Lutgens E, de Muinck ED, Kitslaar PJ, Tordoir JH, Wellens HJ, Daemen MJ. Biphasic pattern of cell turnover characterizes the progression from fatty streaks to ruptured human atherosclerotic plaques. *Cardiovasc Res.* 1999;41:473–479. doi: 10.1016/s0008-6363(98)00311-3
14. Proudfoot D, Skepper JN, Hegyi L, Bennett MR, Shanahan CM, Weissberg PL. Apoptosis regulates human vascular calcification in vitro: evidence for initiation of vascular calcification by apoptotic bodies. *Circ Res.* 2000;87:1055–1062. doi: 10.1161/01.res.87.11.1055
15. Jeong JH, Jin JS, Kim HN, Kang SM, Liu JC, Lengner CJ, Otto F, Mundlos S, Stein JL, van Wijnen AJ, et al. Expression of Runx2 transcription factor in non-skeletal tissues, sperm and brain. *J Cell Physiol.* 2008;217:511–517. doi: 10.1002/jcp.21524
16. Takarada T, Hinoi E, Nakazato R, Ochi H, Xu C, Tsuchikane A, Takeda S, Karsenty G, Abe T, Kiyonari H, et al. An analysis of skeletal development in osteoblast-specific and chondrocyte-specific runt-related transcription factor-2 (Runx2) knockout mice. *J Bone Miner Res.* 2013;28:2064–2069. doi: 10.1002/jbmr.1945
17. Zeng C, McNeil S, Pockwinse S, Nickerson J, Shopland L, Lawrence JB, Penman S, Hiebert S, Lian JB, van Wijnen AJ, et al. Intranuclear targeting of AML/CBFalpha regulatory factors to nuclear matrix-associated transcriptional domains. *Proc Natl Acad Sci U S A.* 1998;95:1585–1589. doi: 10.1073/pnas.95.4.1585
18. Lin ME, Chen T, Leaf EM, Speer MY, Giachelli CM. Runx2 expression in smooth muscle cells is required for arterial medial calcification in mice. *Am J Pathol.* 2015;185:1958–1969. doi: 10.1016/j.ajpath.2015.03.020
19. Lin ME, Chen TM, Wallingford MC, Nguyen NB, Yamada S, Sawangmake C, Zhang J, Speer MY, Giachelli CM. Runx2 deletion in smooth muscle cells inhibits vascular osteochondrogenesis and calcification but not atherosclerotic lesion formation. *Cardiovasc Res.* 2016;112:606–616. doi: 10.1093/cvr/cvw205
20. Sun Y, Byon CH, Yuan K, Chen J, Mao X, Heath JM, Javed A, Zhang K, Anderson PG, Chen Y. Smooth muscle cell-specific Runx2 deficiency inhibits vascular calcification. *Circ Res.* 2012;111:543–552. doi: 10.1161/CIRCRESAHA.112.267237
21. Liu L, Zeng P, Yang X, Duan Y, Zhang W, Ma C, Zhang X, Yang S, Li X, Yang J, et al. Inhibition of vascular calcification. *Arterioscler Thromb Vasc Biol.* 2018;38:2382–2395. doi: 10.1161/ATVBAHA.118.311546
22. Röhl S, Rykaczewska U, Seime T, et al. Transcriptomic profiling of experimental arterial injury reveals new mechanisms and temporal dynamics in vascular healing response. *JVS: Vasc Sci.* 2020;1:13–27.
23. Raaz U, Schellinger IN, Chernogubova E, Warnecke C, Kayama Y, Penov K, Hennigs JK, Salomons F, Eken S, Emrich FC, et al. Transcription factor Runx2 promotes aortic fibrosis and stiffness in type 2 diabetes mellitus. *Circ Res.* 2015;117:513–524. doi: 10.1161/CIRCRESAHA.115.306341
24. Yang S, Quaresma AJ, Nickerson JA, Green KM, Shaffer SA, Imbalzano AN, Martin-Buley LA, Lian JB, Stein JL, van Wijnen AJ, et al. Subnuclear domain proteins in cancer cells support the functions of RUNX2 in the DNA damage response. *J Cell Sci.* 2015;128:728–740. doi: 10.1242/jcs.160051
25. Mika S, Rost B. NMPdb: database of nuclear matrix proteins. *Nucleic Acids Res.* 2005;33(Database issue):D160–D163. doi: 10.1093/nar/gki132
26. Okorokov AL, Rubbi CP, Metcalfe S, Milner J. The interaction of p53 with the nuclear matrix is mediated by F-actin and modulated by DNA damage. *Oncogene.* 2002;21:356–367. doi: 10.1038/sj.onc.1205112
27. Erdemir T, Bilican B, Oncel D, Goding CR, Yavuzer U. DNA damage-dependent interaction of the nuclear matrix protein C1D with Translin-associated factor X (TRAX). *J Cell Sci.* 2002;115(pt 1):207–216.
28. Qiao F, Moss A, Kupfer GM. Fanconi anemia proteins localize to chromatin and the nuclear matrix in a DNA damage- and cell cycle-regulated manner. *J Biol Chem.* 2001;276:23391–23396. doi: 10.1074/jbc.M101855200
29. Wysokinski D, Pawlowska E, Blasiak J. RUNX2: a master bone growth regulator that may be involved in the DNA damage response. *DNA Cell Biol.* 2015;34:305–315. doi: 10.1089/dna.2014.2688
30. Blyth K, Vaillant F, Hanlon L, Mackay N, Bell M, Jenkins A, Neil JC, Cameron ER. Runx2 and MYC collaborate in lymphoma development by suppressing apoptotic and growth arrest pathways in vivo. *Cancer Res.* 2006;66:2195–2201. doi: 10.1158/0008-5472.CAN-05-3558
31. Schnerch D, Lausch E, Becker H, Felthaus J, Pfeifer D, Mundlos S, Engelhardt M, Schwabe M, Wäsch R. Up-regulation of RUNX2 in acute myeloid leukemia in a patient with an inherent RUNX2 haploinsufficiency and cleidocranial dysplasia. *Leuk Lymphoma.* 2014;55:1930–1932. doi: 10.3109/10428194.2013.855310
32. Akech J, Wixted JJ, Bedard K, van der Deen M, Hussain S, Guise TA, van Wijnen AJ, Stein JL, Languino LR, Altieri DC, et al. Runx2 association with progression of prostate cancer in patients: mechanisms mediating bone osteolysis and osteoblastic metastatic lesions. *Oncogene.* 2010;29:811–821. doi: 10.1038/onc.2009.389

33. Liu Y, Drozdov I, Shroff R, Beltran LE, Shanahan CM. Prelamin A accelerates vascular calcification via activation of the DNA damage response and senescence-associated secretory phenotype in vascular smooth muscle cells. *Circ Res.* 2013;112:e99–109. doi: 10.1161/CIRCRESAHA.111.300543
34. Wang X, Li B. Genetic studies of bone diseases: evidence for involvement of DNA damage response proteins in bone remodeling. *Int J Biomed Sci.* 2007;3:217–228.
35. Müller KH, Hayward R, Rajan R, Whitehead M, Cobb AM, Ahmad S, Sun M, Goldberga I, Li R, Bashtanova U, et al. Poly(ADP-Ribose) links the DNA damage response and biomineralization. *Cell Rep.* 2019;27:3124–3138.e13. doi: 10.1016/j.celrep.2019.05.038
36. Shiloh Y. ATM and related protein kinases: safeguarding genome integrity. *Nat Rev Cancer.* 2003;3:155–168. doi: 10.1038/nrc1011
37. Rasheed N, Wang X, Niu QT, Yeh J, Li B. Atm-deficient mice: an osteoporosis model with defective osteoblast differentiation and increased osteoclastogenesis. *Hum Mol Genet.* 2006;15:1938–1948. doi: 10.1093/hmg/ddl116
38. Sepe V, Rampino T, Libetta C. Arterial "inflammaging" drives vascular calcification in children on dialysis. *Kidney Int.* 2019;96:522. doi: 10.1016/j.kint.2019.05.021
39. Robaszkiewicz A, Erdélyi K, Kovács K, Kovács I, Bai P, Rajnavölgyi E, Virág L. Hydrogen peroxide-induced poly(ADP-ribosyl)ation regulates osteogenic differentiation-associated cell death. *Free Radic Biol Med.* 2012;53:1552–1564. doi: 10.1016/j.freeradbiomed.2012.08.567
40. Chow WY, Rajan R, Muller KH, Reid DG, Skepper JN, Wong WC, Brooks RA, Green M, Bihan D, Farndale RW, et al. NMR spectroscopy of native and in vitro tissues implicates polyADP ribose in biomineralization. *Science.* 2014;344:742–746. doi: 10.1126/science.1248167
41. Wang C, Xu W, An J, Liang M, Li Y, Zhang F, Tong Q, Huang K. Poly(ADP-ribose) polymerase 1 accelerates vascular calcification by upregulating Runx2. *Nat Commun.* 2019;10:1203. doi: 10.1038/s41467-019-09174-1
42. Reynolds JL, Joannides AJ, Skepper JN, McNair R, Schurgers LJ, Proudfoot D, Jahnen-Dechent W, Weissberg PL, Shanahan CM. Human vascular smooth muscle cells undergo vesicle-mediated calcification in response to changes in extracellular calcium and phosphate concentrations: a potential mechanism for accelerated vascular calcification in ESRD. *J Am Soc Nephrol.* 2004;15:2857–2867. doi: 10.1097/01.ASN.0000141960.01035.28
43. Orita Y, Yamamoto H, Kohno N, Sugihara M, Honda H, Kawamata S, Mito S, Soe NN, Yoshizumi M. Role of osteoprotegerin in arterial calcification: development of new animal model. *Arterioscler Thromb Vasc Biol.* 2007;27:2058–2064. doi: 10.1161/ATVBAHA.107.147868
44. Verhulst A, Neven E, D'Haese PC. Characterization of an animal model to study risk factors and new therapies for the cardiorenal syndrome, a major health issue in our aging population. *Cardiorenal Med.* 2017;7:234–244. doi: 10.1159/000462984
45. Zhen Y, Yu Y. Proteomic analysis of the downstream signaling network of PARP1. *Biochemistry.* 2018;57:429–440. doi: 10.1021/acs.biochem.7b01022
46. Ding HT, Wang CG, Zhang TL, Wang K. Fibronectin enhances in vitro vascular calcification by promoting osteoblastic differentiation of vascular smooth muscle cells via ERK pathway. *J Cell Biochem.* 2006;99:1343–1352. doi: 10.1002/jcb.20999
47. Xiao G, Jiang D, Thomas P, Benson MD, Guan K, Karsenty G, Franceschi RT. MAPK pathways activate and phosphorylate the osteoblast-specific transcription factor, Cbfa1. *J Biol Chem.* 2000;275:4453–4459. doi: 10.1074/jbc.275.6.4453
48. Willis DM, Loewy AP, Charlton-Kachigian N, Shao JS, Ornitz DM, Towler DA. Regulation of osteocalcin gene expression by a novel Ku antigen transcription factor complex. *J Biol Chem.* 2002;277:37280–37291. doi: 10.1074/jbc.M206482200
49. Xiao A, Li H, Shechter D, Ahn SH, Fabrizio LA, Erdjument-Bromage H, Ishibe-Murakami S, Wang B, Tempst P, Hofmann K, et al. WSTF regulates the H2A.X DNA damage response via a novel tyrosine kinase activity. *Nature.* 2009;457:57–62. doi: 10.1038/nature07668
50. Cook PJ, Ju BG, Telese F, Wang X, Glass CK, Rosenfeld MG. Tyrosine dephosphorylation of H2AX modulates apoptosis and survival decisions. *Nature.* 2009;458:591–596. doi: 10.1038/nature07849
51. Krishnan N, Jeong DG, Jung SK, Ryu SE, Xiao A, Allis CD, Kim SJ, Tonks NK. Dephosphorylation of the C-terminal tyrosyl residue of the DNA damage-related histone H2A.X is mediated by the protein phosphatase eyes absent. *J Biol Chem.* 2009;284:16066–16070. doi: 10.1074/jbc.C900032200
52. Singh RK, Gunjan A. Histone tyrosine phosphorylation comes of age. *Epigenetics.* 2011;6:153–160. doi: 10.4161/epi.6.2.13589
53. Tay LS, Krishnan V, Sankar H, Chong YL, Chuang LSH, Tan TZ, Kolinjivadi AM, Kappei D, Ito Y. RUNX Poly(ADP-Ribosyl)ation and BLM interaction facilitate the fanconi anemia pathway of DNA repair. *Cell Rep.* 2018;24:1747–1755. doi: 10.1016/j.celrep.2018.07.038
54. Zhang Y, Wang J, Ding M, Yu Y. Site-specific characterization of the Asp- and Glu-ADP-ribosylated proteome. *Nat Methods.* 2013;10:981–984. doi: 10.1038/nmeth.2603
55. Ansari B, Coates PJ, Greenstein BD, Hall PA. In situ end-labelling detects DNA strand breaks in apoptosis and other physiological and pathological states. *J Pathol.* 1993;170:1–8. doi: 10.1002/path.1711700102
56. Shroff RC, McNair R, Figg N, Skepper JN, Schurgers L, Gupta A, Hiorns M, Donald AE, Deanfield J, Rees L, et al. Dialysis accelerates medial vascular calcification in part by triggering smooth muscle cell apoptosis. *Circulation.* 2008;118:1748–1757. doi: 10.1161/CIRCULATIONAHA.108.783738
57. Pratap J, Lian JB, Javed A, Barnes GL, van Wijnen AJ, Stein JL, Stein GS. Regulatory roles of Runx2 in metastatic tumor and cancer cell interactions with bone. *Cancer Metastasis Rev.* 2006;25:589–600. doi: 10.1007/s10555-006-9032-0
58. Davie JR. The nuclear matrix and the regulation of chromatin organization and function. *Int Rev Cytol.* 1995;162A:191–250. doi: 10.1016/s0074-7696(08)61232-2
59. Reyes JC, Muchardt C, Yaniv M. Components of the human SWI/SNF complex are enriched in active chromatin and are associated with the nuclear matrix. *J Cell Biol.* 1997;137:263–274. doi: 10.1083/jcb.137.2.263
60. Wu H, Whitfield TW, Gordon JA, Dobson JR, Tai PW, van Wijnen AJ, Stein JL, Stein GS, Lian JB. Genomic occupancy of Runx2 with global expression profiling identifies a novel dimension to control of osteoblastogenesis. *Genome Biol.* 2014;15:R52. doi: 10.1186/gb-2014-15-3-r52
61. Blyth K, Cameron ER, Neil JC. The RUNX genes: gain or loss of function in cancer. *Nat Rev Cancer.* 2005;5:376–387. doi: 10.1038/nrc1607
62. Blyth K, Terry A, Mackay N, Vaillant F, Bell M, Cameron ER, Neil JC, Stewart M. Runx2: a novel oncogenic effector revealed by in vivo complementation and retroviral tagging. *Oncogene.* 2001;20:295–302. doi: 10.1038/sj.onc.1204090
63. Jungmichel S, Rosenthal F, Altmeyer M, Lukas J, Hottiger MO, Nielsen ML. Proteome-wide identification of poly(ADP-Ribosyl)ation targets in different genotoxic stress responses. *Mol Cell.* 2013;52:272–285. doi: 10.1016/j.molcel.2013.08.026
64. Stucki M, Clapperton JA, Mohammad D, Yaffe MB, Smerdon SJ, Jackson SP. MDC1 directly binds phosphorylated histone H2AX to regulate cellular responses to DNA double-strand breaks. *Cell.* 2005;123:1213–1226. doi: 10.1016/j.cell.2005.09.038
65. Lu C, Zhu F, Cho YY, Tang F, Zykova T, Ma WY, Bode AM, Dong Z. Cell apoptosis: requirement of H2AX in DNA ladder formation, but not for the activation of caspase-3. *Mol Cell.* 2006;23:121–132. doi: 10.1016/j.molcel.2006.05.023
66. Pignoni F, Hu B, Zavitz KH, Xiao J, Garrity PA, Zipursky SL. The eye-specification proteins So and Eya form a complex and regulate multiple steps in Drosophila eye development. *Cell.* 1997;91:881–891. doi: 10.1016/s0092-8674(00)80480-8
67. Zhu S, Paydar M, Wang F, Li Y, Wang L, Barrette B, Bessho T, Kwok BH, Peng A. Kinesin kif2c in regulation of DNA double strand break dynamics and repair. *eLife.* 2020;9:e53402.
68. Aguilar-Quesada R, Muñoz-Gámez JA, Martín-Oliva D, Peralta A, Valenzuela MT, Matínez-Romero R, Quiles-Pérez R, Menissier-de Murcia J, de Murcia G, Ruiz de Almodóvar M, et al. Interaction between ATM and PARP-1 in response to DNA damage and sensitization of ATM deficient cells through PARP inhibition. *BMC Mol Biol.* 2007;8:29. doi: 10.1186/1471-2199-8-29
69. Bartoli-Leonard F, Wilkinson FL, Schiro A, Inglott FS, Alexander MY, Weston R. Loss of sirt1 in diabetes accelerates DNA damage induced vascular calcification. *Cardiovasc Res.* 2020:cvaa134. doi: 10.1093/cvr/cvaa134
70. Nadlonek NA, Weyant MJ, Yu JA, Cleveland JC Jr, Reece TB, Meng X, Fullerton DA. Radiation induces osteogenesis in human aortic valve interstitial cells. *J Thorac Cardiovasc Surg.* 2012;144:1466–1470. doi: 10.1016/j.jtcvs.2012.08.041
71. Rosina M, Langone F, Giuliani G, Cerquone Perpetuini A, Reggio A, Calderone A, Fuoco C, Castagnoli L, Gargioli C, Cesareni G. Osteogenic differentiation of skeletal muscle progenitor cells is activated by the DNA damage response. *Sci Rep.* 2019;9:5447. doi: 10.1038/s41598-019-41926-3